

Contents lists available at ScienceDirect

# Petroleum Science

journal homepage: www.keaipublishing.com/en/journals/petroleum-science



# Original Paper

# Low-amplitude structure recognition method based on nonsubsampled contourlet transform



Fen Lyu a, b, d, Xing-Ye Liu a, b, \*, Li Chen a, b, Chao Li a, b, Jie Zhou a, b, Huai-Lai Zhou a, b, c

- <sup>a</sup> Key Lab of Earth Exploration & Information Techniques of Ministry of Education, Chengdu University of Technology, Chengdu, 610059, Sichuan, China
- <sup>b</sup> College of Geophysics, Chengdu University of Technology, Chengdu, 610059, Sichuan, China
- c State Key Laboratory of Oil and Gas Reservoir Geology and Exploitation, Chengdu University of Technology, Chengdu, 610059, Sichuan, China
- <sup>d</sup> Postdoctoral Research Station of the School of Geophysics, Chengdu University of Technology, Chengdu, 610059, Sichuan, China

#### ARTICLE INFO

### Article history: Received 28 July 2023 Received in revised form 6 February 2024 Accepted 28 March 2024 Available online 5 April 2024

Edited by Jie Hao and Meng-Jiao Zhou

Keywords:
Shale gas
Low-amplitude structure
Low-frequency background
Non-subsampled contourlet transform
Horizontal well verification

#### ABSTRACT

Currently, horizontal well fracturing is indispensable for shale gas development. Due to the variable reservoir formation morphology, the drilling trajectory often deviates from the high-quality reservoir, which increases the risk of fracturing. Accurately recognizing low-amplitude structures plays a crucial role in guiding horizontal wells. However, existing methods have low recognition accuracy, and are difficult to meet actual production demand. In order to improve the drilling encounter rate of highquality reservoirs, we propose a method for fine recognition of low-amplitude structures based on the non-subsampled contourlet transform (NSCT). Firstly, the seismic structural data are analyzed at multiple scales and directions using the NSCT and decomposed into low-frequency and high-frequency structural components. Then, the signal of each component is reconstructed to eliminate the low-frequency background of the structure, highlight the structure and texture information, and recognize the lowamplitude structure from it. Finally, we combined the drilled horizontal wells to verify the lowamplitude structural recognition results. Taking a study area in the west Sichuan Basin block as an example, we demonstrate the fine identification of low-amplitude structures based on NSCT. By combining the variation characteristics of logging curves, such as organic carbon content (TOC), natural gamma value (GR), etc., the real structure type is verified and determined, and the false structures in the recognition results are checked. The proposed method can provide reliable information on lowamplitude structures for optimizing the trajectory of horizontal wells. Compared with identification methods based on traditional wavelet transform and curvelet transform, NSCT enhances the local features of low-amplitude structures and achieves finer mapping of low-amplitude structures, showing promise for application.

© 2024 The Authors. Publishing services by Elsevier B.V. on behalf of KeAi Communications Co. Ltd. This is an open access article under the CC BY-NC-ND license (http://creativecommons.org/licenses/by-nc-nd/4.0/).

### 1. Introduction

The increase in shale gas production plays a crucial role in optimizing the energy structure (Qian et al., 2018). Shale, as an integrated reservoir system for production and storage, can only realize its commercial value through horizontal well fracturing technology. Currently, shale gas development primarily relies on horizontal wells in many areas (Xue et al., 2021). In horizontal well

E-mail address: lxylxx@cdut.edu.cn (X.-Y. Liu).

guidance, geophysical data provides valuable insights for macroscopic guidance, while 3D seismic data offers advantages in predicting planar and spatial combinations. However, accurately identifying various low-amplitude structures (such as uplifts, folds, faults, and pop-up structures) solely from the seismic dataset is challenging. Additionally, erroneous impedance interface analysis may lead to the creation of false structures during prediction (Liu et al., 2022a). These factors can result in the deviation of the actual drilling trajectory from the design trajectory or a low drilling encounter rate for high-quality reservoirs. To mitigate errors and losses, it is imperative to conduct research on fine identification of low-amplitude structures without delay. This technology enables accurate identification of genuine geological patterns and types of

<sup>\*</sup> Corresponding author. Key Lab of Earth Exploration & Information Techniques of Ministry of Education, Chengdu University of Technology, Chengdu, 610059, Sichuan, China.

low-amplitude structures, effectively rectifying false structures resulting from erroneous predictions. Additionally, it enables analysis and determination of formation breakpoints, fault distances, the true trend pattern of the formation, and the position of the trajectory relative to the reservoir. Consequently, this method provides robust technical support and ensures effective quality assurance for optimizing and adjusting horizontal well trajectories, thereby enhancing the drilling encounter rate of high-quality reservoirs.

Low-amplitude structures, characterized by gentle geological features and closure amplitudes ranging from 10 to 20 m, are also known as small or micro-amplitude structures (Zhao, 1982, 1987). Despite their importance in the field of oil and gas exploration, the study of low-amplitude structures has only recently garnered attention. The challenges lie in their subtle nature, reflected in seismic data through flat reflection axes and minimal amplitude variations, rendering identification a complex task. The accuracy of interpreting low-amplitude structures hinges on multiple facets of seismic data acquisition, processing, and interpretation. Existing methods for identifying these structures can be categorized into three main groups. The first approach involves establishing a highprecision velocity field through velocity analysis, a crucial parameter in seismic exploration, especially when studying lowamplitude structures. Inaccurate velocity analysis can obscure genuine structures or introduce false ones. Achieving a highly precise interpretation of horizons and faults and employing highprecision velocity fields for time-depth conversion are essential for mapping low-amplitude structures. Wang et al. (2015) and Pu (1998) conducted an analysis of correction methods for lowamplitude structural velocity fields and structural maps using drilling and logging data. Zhang and Huang (2002) proposed the presence of velocity anomalies by selecting different static correction datums. This assertion is based on the premise that, against the backdrop of TO as a wide and gentle platform, a specific threshold of velocity anomaly difference in the up-dip direction is required to generate an anticline shape in that direction. Shao et al. (2003) integrated static correction, correlation processing, and velocity spectrum with interpretation, velocity analysis, and mapping to achieve a comprehensive analysis, ultimately resulting in a structural map with significantly enhanced velocity accuracy. Meanwhile, Teng et al. (2005) utilized P-wave and S-wave velocity models to conduct pre-stack Kirchhoff integral migration on 2D seismic data, obtaining depth and time profiles of various P-wave and converted S-wave components, and subsequently performing joint interpretation of minor faults and low structures based on these findings. Zhou et al. (2006) proposed the utilization of the average velocity change method for the analysis of stacking velocity and velocity within layers. Based on this approach, the correction of velocities using VSP velocity can enhance the resolution of both vertical and horizontal velocities. Taking into account the velocity mapping characteristics in the southern margin of the Junggar Basin, Xu et al. (2012) applied the standard layer correction velocity anomaly method to eliminate the influence of seismic anomaly spectrum points and improve the quality of seismic velocity. This improvement resulted in a more reliable structural map for oil and gas exploration purposes. Wang et al. (2015) conducted seismic data reprocessing and interpreted and analyzed the data volumes processed by various methods. Through refined velocity analysis, the low-amplitude structure of the Matouying uplift was reimplemented using variable-velocity mapping technology. Building upon the full application of the stacking velocity spectrum and incorporating well point velocity correction and stratigraphic control methods, Zheng et al. (2017) accurately characterized shallow low-amplitude structures by finely adjusting the average velocity field in the area. To address the challenge of long wavelength static correction in complex surface areas, Wang et al. (2018) employed a layered constraint modeling approach for layered constraint tomography inversion near-surface modeling. This enabled the identification of low-amplitude structures. Finally, Hu et al. (2019) proposed the utilization of stratified fitting to obtain layer velocities and establish the average velocity field. This approach allowed for the reliable identification of low-amplitude structures above 3 m through the creation of a large-scale structural map.

However, the aforementioned methods based on velocity analysis still have many deficiencies. First, there are many causes of velocity variation (Liu et al., 2020, 2021), including formation lithology, burial depth, thickness variation, formation combination, denudation, surface velocity anomaly, formation porosity, fluid properties, etc. Therefore, it is difficult to accurately establish the three-dimensional velocity field with large velocity variation, which leads to distortion, large calculation, and high cost. Secondly, with the continuous improvement in the accuracy requirements for characterizing low-amplitude structures, the previous structure map was prepared by time-depth conversion using a single velocity gauge plate with points instead of surfaces. This method often ignores the spatial variation of formation velocity, resulting in low accuracy of structure mapping and deviation of trap implementation, which leads to drilling failure. Thirdly, the method cannot describe the overall trend of low-amplitude structure systematically. Therefore, to further improve the accuracy of low-amplitude structure prediction and better analyze the trend surface background, some scholars applied the trend surface analysis to the low-amplitude structure identification technique. Lancaster and Salkauskas (1981) introduced the moving trend surface method for detecting low-amplitude structures. Jiang et al. (2005) proposed a methodology involving fine structural mapping, subtraction of regional structural trend backgrounds to derive residual structural maps in complex structural settings, and subsequent analysis of low-amplitude structures. Ge and Kang (2008) incorporated a weighted term into the trend surface analysis algorithm to account for varying distance effects on interpolation points. Mullineux (2008) advocated for a least-squares fit approach to layering and investigated the behavior of fitting coefficients. Fang et al. (2010) enhanced the accuracy of identifying low-amplitude structures by integrating the coherence cube, slicing, structural residual, and integral seismic trace methods. Hu et al. (2012) utilized seismic, logging, and other datasets to detect and explore low-amplitude structural traps through trend surface analysis, isochronal slicing, coherent body, and fine-scale mapping of well-point data. Li et al. (2016) developed a three-dimensional dynamic trending method based on the original two-dimensional moving trend surface method, applied notably in ground subsidence analysis. Wu et al. (2017) iteratively applied the moving trend surface method to identify low-amplitude structures. Through the selection of quadratic fitting and optimization of sampling intervals and influence radii, they determined the most effective parameter combination for such identification. Chai and Bi (2019) employed a twodimensional trend surface technique to identify low-amplitude structures in areas characterized by steep dip angles of the strata. He and Chen (2020) utilized the phase-body constraint method for detailed layer interpretation following meticulous processing of original seismic data, successfully pinpointing low-amplitude structures. Zhu et al. (2020) proposed a true-false low-amplitude structural analysis and identification technique based on trend surface analysis, enabling precise recognition of genuine lowamplitude structural configurations and types. However, the trend surface analysis method relies too much on the structural background data, which results in a low-amplitude structure "illusion" and affects the recognition effect. At the same time, the

method is affected by many vital parameters, and the optimal parameter combination for different work areas requires repeated experiments, resulting in low efficiency. Moreover, the method only considers the two-dimensional horizon information. It cannot explore the rich structural information in the three-dimensional seismic data, resulting in a limited agreement between the recognition results and the drilled wells.

The traditional method of low-amplitude structure identification is difficult, mainly because the structure background frequency band is multiple, which affects the judgment of low-amplitude structure. The time-frequency analysis technique can well describe the variation pattern of structure signal frequency, i.e., meticulously portray the characteristics and properties of various types of structures in the data, visually identify, examine and classify the data, separate the low-frequency information reflecting the large background of structures, and enhance the information of low-amplitude structure frequency band. Therefore, in recent years, scholars have made efforts to identify low-amplitude structures through time-frequency analysis, yielding promising outcomes. For instance, Bai et al. (2011) established a seismic cycle characteristic model and an S-domain time-frequency response model for representative sedimentary cycles. Concurrently, they created a precise isochronous sedimentation grid for the entire study area through the joint calibration of 2D spectra and singlewell sedimentation cycles. This grid facilitated the detailed tracing of low-amplitude structures. Xia et al. (2021) employed the trend decomposition method to map low-amplitude structures by identifying inflection points of structural fluctuations and combining them with wavelet decomposition to generate interpretation maps. Wu et al. (2022) enhanced data resolution and accuracy in imaging low-amplitude structures by employing nearsurface Q compensation and robust deconvolution techniques. However, these methods primarily analyze at a single scale, lacking detailed decomposition and highlighting of different frequency components. Consequently, they fail to address structural intricacies, such as subtle fluctuations in the structure map, resulting in low recognition accuracy, multiple spurious images, and limited sensitivity to low-amplitude structures.

Based on previous methods in time-frequency analysis for identifying low-amplitude structures, we have taken into account the characteristics of low-frequency smoothing and local highfrequency fluctuations within these structures. Our proposal involves a multi-scale recombination of the low-frequency and highfrequency components of the structure, aiming to enhance the weight of high-frequency components in the identification process while reducing the masking effect of low-frequency components. To achieve this, we have conducted an extensive study on the multi-scale analysis method. One commonly employed technique in multi-scale time-frequency analysis is wavelet transform, which has found wide application in signal processing, image processing, compression coding, and other related fields. The concept of wavelet transform was initially introduced by the French mathematicians Grossmann and Morlet (1984). It utilizes wavelet basis functions with variable scales and translation parameters for signal analysis. Therefore, the careful selection of appropriate wavelet basis functions is crucial for effectively identifying low-amplitude structures. Various wavelet basis functions offer different timefrequency resolutions and smoothness, and the improper choice of these functions may lead to inadequate identification of lowamplitude structures. To overcome the limitations of wavelet transform in processing two-dimensional signals, American mathematicians Candes and Donoho (1999) proposed curvelet decomposition as a curve-based representation method based on multi-scale and multi-directional analysis. Herrmann et al. (2008) applied this method to seismic signal research, achieving robust separation of primary and multiple reflections in the curvelet domain. Compared to wavelet transform, the decomposition coefficients of curvelet transform provide a better reflection of the local features of signals and images, effectively capturing the characteristic information of low-amplitude structures. However, the performance of curvelet transform is greatly influenced by parameter selection, such as thresholding of curvelet coefficients. scale, and direction selection. Moreover, curvelet transform is sensitive to noise when identifying low-amplitude structures, which can easily lead to misjudgment or over-interpretation. In an effort to further overcome the limitations of traditional multi-scale analysis methods in image processing, Do and Vetterli (2002) proposed contourlet transform, which inherits the idea of multiscale analysis and introduces the multi-scale analysis characteristics of curves and surfaces. This method can accurately capture the microstructure information of images, thereby improving their resolution and representation capability. Asmare et al. (2015) found that the basis functions used in contourlet transform possess higher direction selectivity and spatial locality, making them better suited for capturing the local characteristics of low-amplitude structure signals. Furthermore, this method provides better resolution at different scales, enabling a more accurate description of the multiscale features within low-amplitude structures.

Therefore, by extensively referring to previous research methods, we propose the adoption of a de-low frequency approach. This method entails decomposing the structural travel time data into details and trends (also referred to as low-frequency background) using the non-subsampled contourlet transform method. Through this process, the slope background or complex structural background becomes more horizontal. The proposed method analyzes the characteristics of micro amplitude structures across multiple scales and directions. By reducing the low-frequency components, this approach mitigates the influence of regional structural morphology and eliminates interference from different structural backgrounds when interpreting low-amplitude structures. It effectively highlights the nuanced changes in local structures, rendering their morphology more visually comprehensible. Ultimately, this approach enhances the accuracy and reliability of low-amplitude structure recognition.

### 2. Methodology

We utilize three methods for decomposing the data of structural interpretation, thereby separating it into two components: the structural background and the low-amplitude structural details. Through this process, the influence of the structural background is attenuated while the local low-amplitude structural features are enhanced, enabling the effective highlighting of low-amplitude structures. This "de-low frequency" procedure is visualized in Fig. 1. The three employed methods encompass wavelet

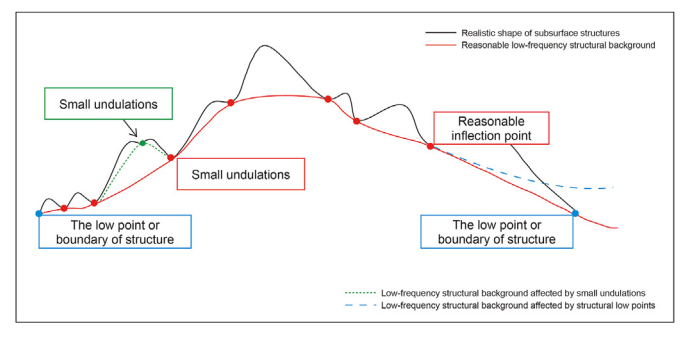


Fig. 1. Illustration of the "de-low frequency" process.

decomposition, curvelet decomposition, and the non-subsampled contourlet decomposition method.

#### 2.1. Wavelet decomposition

Wavelet transform is a multi-scale analysis method that inherits and expands on the idea of short-time Fourier transform localization. It overcomes the limitations of fixed window size with frequency and provides a 'time-frequency' window that varies with frequency. This method has the ability to fully accentuate certain aspects of the problem through the transform, localize time (or space) frequency analysis, and gradually refine the signal (or function) through scaling and translation operations across multiple scales. With this approach, high frequencies can be subdivided into smaller frequency bands while low frequencies can be coarsely subdivided, automatically adapting to the requirements of time-frequency signal analysis to focus on any details of the signal. Additionally, the method allows for obtaining the low-frequency structure background (Shang and Caldwell, 2003; Schonewille et al., 2007).

The 2D wavelet forward transform formula can be expressed as

$$S(b,c,a) = \frac{1}{a} \int_{-\infty}^{+\infty} \int_{-\infty}^{+\infty} g_x \left( \frac{x-b}{a} \right) \cdot g_y \left( \frac{y-c}{a} \right) f(x,y) dxdy \tag{1}$$

where a is the scale parameter, b and c are the plane position parameters along the x and y directions, f(x,y) represents the construction travel time interpretation horizon data,  $g_x\left(\frac{x-b}{a}\right)$  is the wavelet function along the x direction, and  $g_y\left(\frac{y-c}{a}\right)$  is the wavelet function along the y direction.

After performing a 2D wavelet multi-scale analysis on the interpreted travel time data, we select the large-scale data for 2D wavelet inverse transformation to derive the construction background. The equation for the 2D wavelet inverse transformation is as follows:

$$f(x,y) = \frac{1}{C_g} \int_0^{+\infty} \frac{\mathrm{d}a}{a^3} \iint S(b,c,a) \cdot g_x \left(\frac{x-b}{a}\right) g_y \left(\frac{y-c}{a}\right) \mathrm{d}b \mathrm{d}c \tag{2}$$

$$C_{g} = \frac{1}{4\pi^{2}} \iint \frac{\left|G_{g}(w_{1}, w_{2})\right|^{2}}{\left|w_{1}^{2} + w_{2}^{2}\right|} dw_{1} dw_{2}$$
(3)

where  $C_g$  is the Fourier transform of the wavelet function, and  $G_g$  is the Fourier transform of g.

The process of structural recognition through wavelet decomposition involves the manual selection of appropriate scale parameters and the utilization of 2D wavelet transform technology to conduct multi-scale analysis on structural interpretation horizon data, resulting in the extraction of low-frequency (multi-scale) structural backgrounds. This separation effectively isolates the background from local details (small-scale structures), achieving the objective of accentuating low-amplitude details. By fully utilizing the time-frequency characteristics of wavelet decomposition, different frequency components are decomposed and emphasized, enabling the focus on specific details such as small fluctuations within the entire structural map. Ultimately, a de-low-frequency, low-amplitude structural map is obtained, capable of highlighting changes in detail (Bai et al., 2011).

## 2.2. Curvelet decomposition

Although the wavelet coefficient scaling presented by Donoho (1995) has been extensively utilized, it can only display "over"

edge information and not "along" edge information when processing 2D images. Thus, Emmanuel and Donoho (2000) proposed the curvelet transform based on their research on the ridgelet transform. The first-generation curvelet is a multi-scale ridgelet transform that initially divides the image into subbands of diverse scales using filters. Afterwards, edge and noise information can be distinctly separated on different subbands, and the ridgelet transform is applied to each block after dividing the subbands. However, the first-generation curvelet transform requires spatially positioned multi-scale windows and overlapping to prevent block effects, leading to redundancy. To overcome these limitations, Candes and Donoho (2010) proposed a new curvelet compact framework that directly performs multi-scale analysis from the frequency domain, similar to the first-generation algorithm's anisotropic scale relations. This new framework accurately reconstructs the object and is called the second-generation curvelet transform.

The second-generation curvelet framework reduces the number of parameters used in previous curved wave implementation methods, and its parameters are  $\mu(j,l,k)$ , where j is the scale parameter,  $j=0,1,2,\cdots,l$  represents the direction parameter, k is the position parameter. The reduction of parameters facilitates the computational analysis. The second-generation curvelet transform can be expressed as the inner product of the basis function and the signal (or function) in the same way as the wavelet transform, as follows:

$$C(j,l,k) \stackrel{\text{def}}{=} \langle f, \varphi_{i,l,k} \rangle \tag{4}$$

$$C(j,l,k) \stackrel{\text{def}}{=} \left[ \widehat{f} \overline{U}_j(\omega) e^{i\langle b,\omega \rangle} d\omega \right]$$
 (5)

where  $\varphi_{j,l,k}$  is the curvelet function.

There are two discrete digital implementations of the second-generation curvelet transform, unequally-space fast Fourier transform (USFFT) and wrapping. The main difference between the two methods is the different processing methods for each pair of scale and angle (j,l) unit space.

Given the known object  $f \in \mathbb{R}^2$ , the USFFT is implemented by the following steps:

- (1) Perform a 2D Fourier transform on f to obtain the Fourier sampling set  $\widehat{f}(n_1, n_2), -\frac{n}{2} \le n_1, n_2 \le \frac{n}{2}$ ;
- (2) For each pair of scales and angles (j,l),  $\widehat{f}(n_1,n_2)$  is resampled (or interpolated) as  $\widehat{f}(n_1,n_2-n_1\tan\theta_l)$ ;
- (3) Multiply  $\hat{f}$  with fitting window  $\hat{U}(n_1, n_2)$  to obtain  $\tilde{f}$ ;
- (4) Perform a 2D inverse Fourier transform to obtain the curvelet coefficient  $c^{D}(j,l,k)$ .

Given the object  $f \in \mathbb{R}^2$ , Wrapping is divided into the following four steps:

- (1) Perform a 2D Fourier transform on a to obtain the Fourier sampling set  $\widehat{f}(n_1, n_2), -\frac{n}{2} \le n_1, n_2 \le \frac{n}{2}$ .
- (2) Calculate the product  $\tilde{U}(n_1, n_2)\hat{f}(n_1, n_2)$  in units of each pair of scales and angles (j, l).
- (3) Transform the above product  $\tilde{f}(n_1,n_2)=W(\tilde{U}_{j,l}\hat{f})(n_1,n_2), 0 \le n_1 \le L_1, 0 \le n_2 \le L_2.$
- (4) Perform a 2D inverse Fourier transform on  $\tilde{f}$  to obtain the curvelet coefficient  $c^{D}(j,l,k)$ .

Based on this, we select the wrapping method to implement the

curvelet, take the construction interpretation horizon data as a function f, and then perform the inner product with the curvelet function  $\varphi_{j,l,k}$  to obtain the curvelet coefficients C(j,l,k) at different scales. The processed structural region information and detail information (low-amplitude structure) can be obtained by processing the curvelet coefficient and reconstructing the inverse curvelet transform.

# 2.3. Non-subsampled contourlet decomposition

The 2D separable wavelet transform, an extension of the commonly used 1D wavelet transform, exhibits significant limitations in capturing the edge geometric features of 2D images. This is primarily due to the limited directionality of the extended 2D wavelet transform, rendering it inadequate as a true 2D wavelet transform. To overcome these limitations, Lu and Do (2003) introduced the contourlet transform as a novel tool for multiscale geometric analysis. Unlike the 2D wavelet transform, the contourlet transform not only retains the key features of wavelets, such as multiscale and time-frequency localized distribution properties but also exhibits a high degree of directionality and anisotropy. This enables a varied and adaptable number of directional decompositions at each scale. Consequently, the contourlet transform can effectively decompose different frequency components of actual structural data, enabling a focused representation of structural details such as minor undulations, ultimately highlighting low-amplitude structures.

The non-subsampled contourlet transform (NSCT) is an extension of the contourlet transform (Cunha et al., 2005) that enables multi-scale and multi-directional image decomposition. It was developed to address the issue of frequency aliasing caused by the up-sampling and down-sampling operations in the contourlet transform during image decomposition and reconstruction (Zhang and Guo, 2007). Due to its exceptional characteristics, NSCT has found wide applications in image denoising (Cunha et al., 2006), image enhancement (Zhou et al., 2005), and image fusion, establishing itself as one of the most effective image fusion algorithms.

Similar to wavelet variations, NSCT comprises two main components: the forward transform and the inverse transform, as illustrated in Fig. 2. The forward transform involves decomposing the source image, while the inverse transform reconstructs the source image using the sub-band images obtained from the decomposition. Both the decomposition and reconstruction processes of NSCT are based on the non-subsampled pyramid (NSP) and non-subsampled directional filter bank (NSDFB). The NSP accomplishes the multi-scale decomposition (reconstruction), while the NSDFB achieves the multi-directional decomposition (reconstruction) of the image. These processes share the same basic principles.

Taking the forward transform process of NSCT as an example, the NSCT decomposition process is shown in Fig. 3. It can be seen that the NSCT decomposition structure in the figure consists of two main parts: non-downsampling pyramid decomposition and non-downsampling directional decomposition. Multi-resolution feature extraction is performed on the constructed image of size  $M \times M$  in a layer, and the constructed image is decomposed into high-frequency and low-frequency components. The obtained

high-frequency components continue to be directionally filtered, while the low-frequency components continue to be decomposed by the pyramid filter NSP in the following scale iteration until the set number of decomposition layers is reached. Taking the two-scale and two-direction decomposition as an example, the framework of its decomposition structure is shown in Fig. 3.

To ensure that NSCT possesses multi-scale characteristics, a dual-channel nonsubsampled filter bank is adopted in the NSP of NSCT. The dual-channel nonsubsampled pyramid filter bank in NSCT is represented by  $\{h_0, h_1, g_0, g_1\}$ , where  $\{h_0, h_1\}$  denotes the decomposition filter bank,  $h_0$  is the low-pass filter, and  $h_1$  is the high-pass filter. Similarly, the reconstruction filter bank is denoted by  $\{g_0,g_1\}$ , where  $g_0$  and  $g_1$  represent the low-pass and high-pass filters. The  $\{h_0, h_1, g_0, g_1\}$  filter bank acts as the prototype filter for the nonsubsampled pyramid transform in NSCT. The filters used for the kth layer (k = 2, 3, 4, ...) pyramid decomposition in the image decomposition stage of NSCT are obtained by upsampling the prototype filters  $h_0$  and  $h_1$  (with zero-padding). The size of the pyramid filters is doubled at each layer. The reconstruction stage follows the same principle (Eq. (6)). It is important to note that these filter banks must satisfy the perfect reconstruction condition, as illustrated in Fig. 4.

$$H_0(z)G_0(z) + H_0(z)G_0(z) = 1$$
 (6)

In each level of the pyramid decomposition, the image is decomposed into high-frequency and low-frequency subband images. Furthermore, through iterative processes, the obtained low-frequency subband images are subjected to the same pyramid decomposition. Therefore, k-level pyramid decomposition generates k+1 subband images, including k high-frequency subbands and one low-frequency subband image, all of which have the same size as the source image. Fig. 5 is a schematic diagram of a three-level pyramid decomposition for constructing an image. In this figure,  $H_0\left(Z^{2^{kl}}\right)$  (k=0,1,2) represents the low-pass filter bank, k denotes the number of decomposition layers, and the gray area represents the frequency passband of each level of pyramid decomposition.

During the process of non-subsampled pyramid decomposition of an image, the ideal frequency support interval of the low-pass filter for the kth layer pyramid decomposition is  $[-(\pi/2^k),\pi/2^k]^2$ , and the ideal frequency support interval of the high-pass filter is also  $[-(\pi/2^{j-1}),(\pi/2^{j-1})]^2/[-(\pi/2^j),(\pi/2^j)]^2$ . Generally, upsampling the pyramid filter of the current level can provide the pyramid filter used in the next level. The definition of the non-subsampled pyramid filter for the kth layer is as follows:

$$H_n^{eq}(z) \begin{cases} H_1\left(Z^{2^{n-1}}\right) \prod_{k=0}^{n-2} H_0\left(Z^{2^k}\right), 1 \le n \le 2^k \\ \prod_{k=0}^{n-2} H_0\left(Z^{2^k}\right), n = 2^k \end{cases}$$
 (7)

where  $Z^k$  represents  $[Z_1^k, Z_2^k]$ .

Different from other image single decomposition methods, in

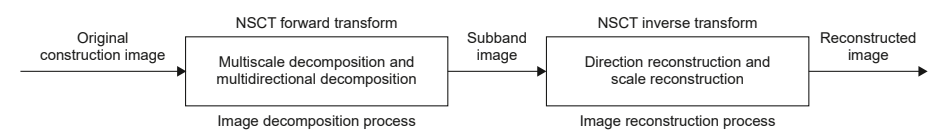


Fig. 2. The NSCT flow diagram of low-amplitude structure recognition in this research.

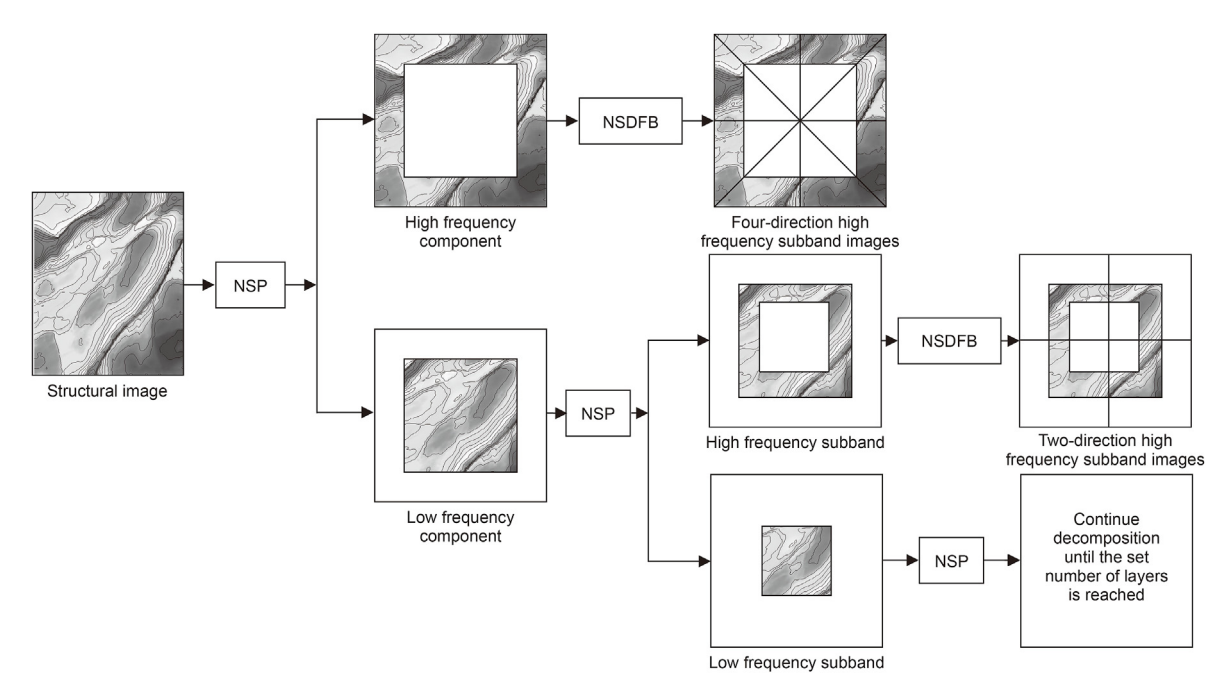


Fig. 3. Schematic diagram of low-amplitude structure identification using NSCT decomposition.

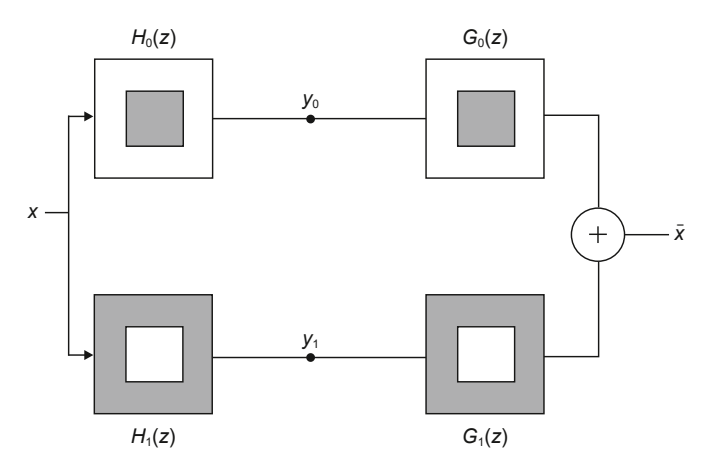


Fig. 4. The ideal NSP filter.

order to obtain rich structural information, we continue to use a NSDFB composed of a two-channel fan filter bank and a plum matrix for two-stage directional filtering superposition for the high-frequency components obtained from the decomposition in Fig. 3. The four-channel filtering structure and the filtering frequency domain distribution are shown in Fig. 6. The first stage is a fan filter bank, which first filters the high-frequency components in the vertical  $U_0(z)$  and horizontal  $U_1(z)$  directions, and then sends the filter results to the second stage quadrant filter. The overlap with the direction of each quadrant filter is the frequency domain distribution of the directional sub-map. The directional sub-map of the overlap area  $y_k$  is output to complete the directional filtering process. After filtering, the high-pass component of each scale is decomposed into  $2^{b_i} (i = 1, 2, \dots, a)$  directional sub-band images, with i being the number of decomposition layers and  $b_i$  being the number of high-frequency subband filtering directions in the current layer. The frequency domain distribution in each direction is shown in Fig. 6(b).

The output equivalent formula of the filter structure can be expressed as

$$y_k: U_k^{\text{eq}}(z) = U_i(z)U_k(z^{\mathbb{Q}}), (i = 0, 1; k = 0, 1, 2, 3)$$
 (8)

where  $y_k$  is the output sub-band in the k direction, corresponding to each labeled frequency band in the filtered partition diagram,  $U_k(z^{\mathbb{Q}})$  represents the sector filtering in the k direction, and  $U_k(z^{\mathbb{Q}})$  represents the quadrant filtering in the k direction. Through the above operation, the direction filter group obtains  $1+\sum_{i=1}^a 2^{b_i} (i=1,2,\cdots,a)$  sub-band images with the same size as the input structure image after completing directional filtering on each decomposition layer. Each decomposition sub-image has anisotropy, thus capturing the structural features of each direction of the structure plane more comprehensively and providing richer structural information for reconstruction after separation.

# 2.4. Comparison of three decomposition methods

The aforementioned wavelet transform, curvelet transform, and NSCT are commonly used transformation methods in signal analysis. They all rely on the principle of multi-scale analysis, allowing for the decomposition and reconstruction of signals at varying scales. In the following analysis, we will assess the strengths and weaknesses of these three methods using mathematical formulas, thereby providing theoretical support for comparing the outcomes obtained by applying these methods to identify low-amplitude structures in practical engineering scenarios.

The wavelet transform is a mathematical tool used for signal and image analysis, providing a multi-resolution representation by decomposing signals or images into subbands of different frequency ranges. Unlike the Fourier transform, the wavelet transform offers a more refined time-frequency analysis and performs better when dealing with non-stationary signals or images. The basic form

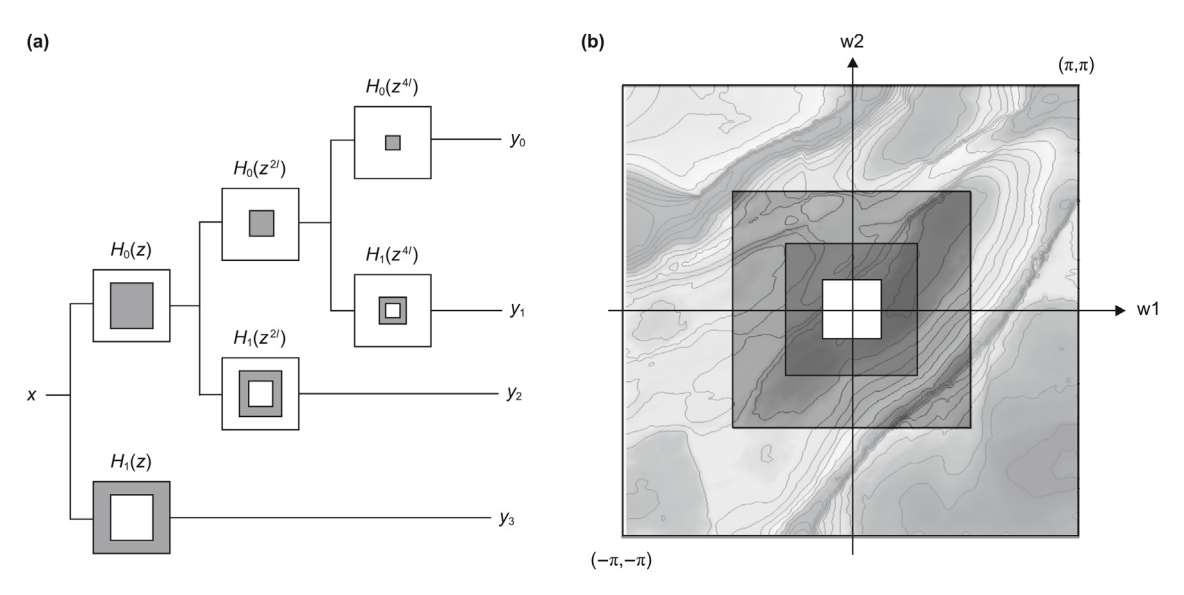


Fig. 5. NSP: (a) three-layer pyramid decomposition structure and (b) frequency domain distribution.

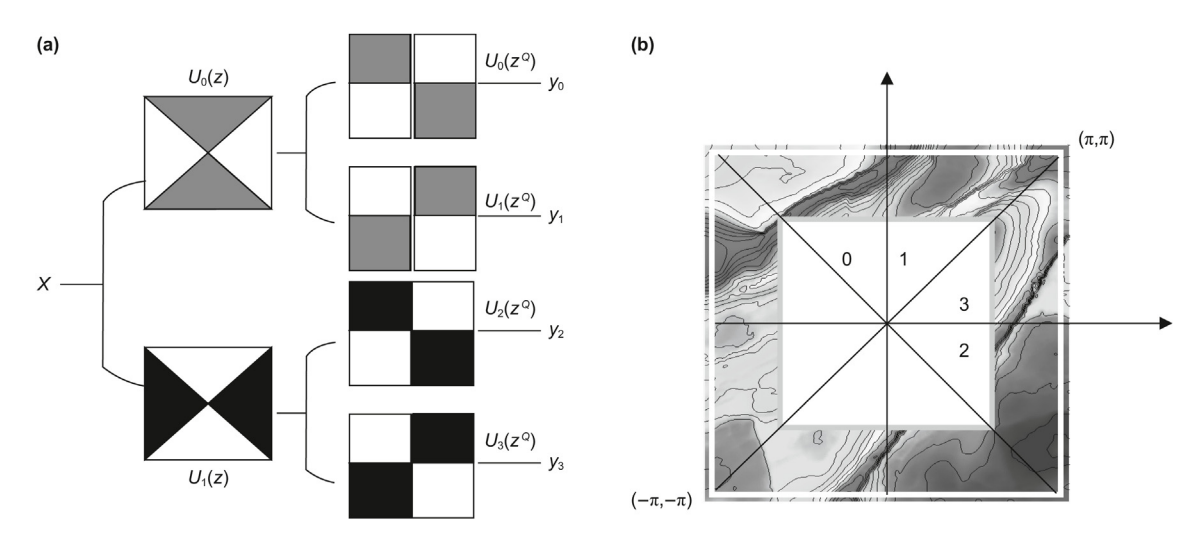


Fig. 6. NSDFB: (a) four-channel directional filter structure and (b) frequency domain distribution.

of the wavelet transform can be represented by the following mathematical formula:

$$W(a,b) = \int_{-\infty}^{\infty} x(t)\psi_{a,b}(t)dt$$
 (9)

where x(t) denotes the input signal,  $\psi_{a,b}(t)$  represents the mother wavelet function, and a and b are scale and shift factors, respectively.

The advantages of wavelet transform can be discerned from the formulas: through adjustment of the scale parameter a, wavelet transform is capable of analyzing signals at varying time or frequency resolutions, thus allowing for the simultaneous provision of time and frequency information and facilitating multi-scale analysis. Moreover, wavelet function  $\psi(t)$  exhibits local properties in both the time and frequency domains, signifying that it has nonzero values within specific ranges. This characteristic implies that wavelet transform is adept at capturing the local features of a signal in time and frequency without being affected by overall signal interference. Nevertheless, the limitations of wavelet transform can

also be deduced from the aforementioned formulas. The selection of wavelet function significantly influences the results of wavelet transform, yet there exists no unified standard or rule for choosing the most suitable wavelet function. Different types of wavelet functions demonstrate diverse frequency characteristics and time-domain responses. Consequently, the selection of an appropriate wavelet function in practical applications often relies on experience or specific problems, involving a degree of subjectivity. Additionally, wavelet transform is sensitive to signal boundaries, potentially leading to the appearance of unnecessary artifacts or distortions at these boundaries.

The curvelet transform is a multiscale analysis method used in signal and image processing, capable of capturing and representing signal features with curved structures and local directionality. As an extension and improvement upon the wavelet transform, it exhibits superior performance in handling signals and images with curved and singular characteristics. These advantages can be explained through mathematical formulae and transformation properties:

$$C(u,v) = \sum_{j,k,l} \psi_{jkl}(u,v)\alpha_{jkl}$$
(10)

where C(u,v) represents the coefficients obtained after the curvelet transform,  $\psi_{jkl}(u,v)$  denotes the curvelet function of the l th ridgelet wavelet in the jth layer and the kth small area, and  $\alpha_{jkl}$  corresponds to the associated coefficients.

In this equation, we can observe that the curvelet transform possesses a multiscale property by employing a multilevel decomposition approach to decompose the signal into different scales of subbands. Each layer of small regions utilizes the same number of curvelet functions, and the boundaries of each region are smooth. Consequently, the curvelet transform is capable of effectively capturing both local and global features of the signal. Furthermore, the curvelet transform exhibits a directional property by adopting the concept of ridgelet waves, constructing a set of basis functions with different directions using orthogonal wavelets within small regions. These basis functions can effectively capture various directional features in the signal, including edges and textures. Moreover, the curvelet transform demonstrates sparsity, representing the signal with a small number of non-zero coefficients, which contributes to its good sparsity property. Due to the localized characteristics of curvelet functions, the curvelet transform can accurately represent the signal with fewer coefficients. However, from the equation, we can also identify the limitations of the curvelet transform. Its performance heavily relies on the selected parameters, such as scale and direction divisions. Choosing inappropriate parameters may lead to inaccurate results. However, the specific mathematical formulas cannot directly indicate how to select these parameters in practical applications; instead, they require empirical and experimental support. Additionally, when dealing with translation-invariant signals, the curvelet transform may result in information loss. Its basis functions are localized in the spatial frequency domain, making it less precise for representing translation-invariant structures.

The NSCT is a multi-scale transformation method based on the NSP and the NSDFB. It is used for image processing and analysis. Given a two-dimensional discrete image f(m,n), NSCT can be represented as follows:

$$NSCT(f)(a,b,\theta,s) = \sum_{m=0}^{M-1} \sum_{n=0}^{N-1} f(m,n) \varphi_{a,b}(m,n) \psi_{\theta,s}(m,n)$$
 (11)

where (a,b) represents the translation parameter,  $\theta$  represents the rotation angle, and s represents the scale parameter. The function  $\varphi_{a,b}(m,n)$  denotes the filter response of the non-subsampled pyramid, which is used for scale decomposition of the signal. The function  $\psi_{\theta,s}(m,n)$  represents the filter response of the NSDFB, which is used for directional decomposition of the signal.

The mathematical expression of NSCT comprises two essential elements: NSP and NSDFB. NSP is a multi-scale decomposition method employed to decompose signals or images into different scale bands. Within the context of NSCT, NSP is utilized for scale decomposition of signals. On the other hand, NSDFB represents a set of filters used to decompose signals in different directions. The combination of these two elements forms the fundamental principle of NSCT.

Therefore, from the aforementioned expression, we can observe that NSCT possesses the following advantages: Firstly, NSCT is capable of providing a multi-scale representation of images, capturing features at different scales. By employing NSP and NSDFB, NSCT effectively handles details and edge information in images. Secondly, NSCT utilizes NSDFB to extract directional features from

images, enabling the analysis of textures and structures in different directions. This gives NSCT an advantage when processing images with prominent directional characteristics, such as textures and edges. Additionally, NSCT adopts a non-subsampled approach for image decomposition, eliminating the need for traditional subsampling operations and thereby preserving more image information, ultimately enhancing the quality of reconstructed images. Moreover, due to its ability to retain more image detail information. NSCT improves the quality of reconstructed images. Lastly, NSCT exhibits a certain degree of noise robustness. Through its multiscale decomposition and direction selectivity, NSCT reduces the impact of noise on images and further attenuates noise during the reconstruction process through filtering operations. However, this method also presents certain limitations. Firstly, it incurs high computational complexity, particularly when processing largersized images. The execution of multi-level pyramid decomposition and directional filtering in NSCT results in significant computational overhead, limiting its practical applicability. Furthermore, parameter selection in NSCT is relatively challenging, requiring empirical knowledge and experimentation to determine appropriate filter choices and pyramid levels. Different images and application scenarios may demand different parameter settings, thereby increasing the difficulty of parameter tuning in NSCT.

In summary, from a theoretical perspective, the wavelet transform, curvelet transform, and NSCT each have their own advantages and limitations when applied to low-amplitude structure recognition. The wavelet transform can effectively extract texture information and edge features of structures, offering certain advantages for structures with prominent frequency domain characteristics. However, its weakness lies in the relatively weak handling of directional features of images, potentially resulting in suboptimal performance when dealing with low-amplitude structures exhibiting clear directional characteristics. The curvelet transform can provide a more accurate description of the geometric structure and edge features of an image, thereby presenting advantages for lowamplitude structures with complex geometric forms. Nevertheless, the curvelet transform also suffers from high computational complexity and sensitivity to parameter settings, requiring finetuning for optimal results. NSCT, on the other hand, can simultaneously consider the multi-scale and multi-directional features of an image, offering advantages for low-amplitude structures with rich textures and complex structures. However, its high computational complexity, challenging parameter selection, and requirement for substantial storage space limit its practical application. Therefore, in practical applications, we choose an appropriate method based on the specific characteristics and requirements of the low-amplitude structure, and conduct a comprehensive comparative analysis of the recognition performance of the three methods to achieve better low-amplitude structure recognition

# 2.5. Workflow of the low-amplitude structure recognition

We use time-frequency analysis techniques to decompose the structural interpretation data from different perspectives and then divide it into the structural background and low-amplitude structural details. Ultimately, the influence of the structural background is weakened, local low-amplitude structural features are enhanced, and low-amplitude structures are revealed. The traditional time-frequency analysis techniques mainly include wavelet, and curvelet transform. In this section, we review the theory of these transform methods. Subsequently, we introduce the NSCT for identifying low-amplitude structures, leveraging its potential in multi-scale and multi-directional analyses. Finally, we delineate the method for identifying low-amplitude structures based on time-

frequency analysis. The technical workflow diagram is illustrated in Fig. 7.

# 3. Application example

#### 3.1. Geological settings

In recent years, a comprehensive study on shale gas genesis and geological conditions in China has determined that shale gas production in the Sichuan Basin is primarily concentrated in the Ordovician Wufeng Formation and Silurian Longmaxi Formation. Current research has made significant progress in the middle and shallow layers, which have burial depths of less than 3500 m (Liu et al., 2023b). However, deep shale gas research has yet to meet commercial development standards, despite extensive research indicating that the development potential of deep shale gas is approximately twice that of the middle and shallow layers. To investigate this further, we selected a study area in the western Chongging block of the Sichuan Basin where the producing formation is buried more than 3500 m deep, as shown in Fig. 8(a). We began by studying the structural, seismic, and logging response characteristics in the study area, following which we carried out low-amplitude structure fine identification to adjust the drilling trajectory (Zhu et al., 2020). The recognition results formed the foundation for subsequent shale gas high-quality reservoir prediction.

The Huangguashan anticline, located in the study area, exhibits an average elevation ranging from 300 to 600 m (Fig. 8(b)). The maximum elevation difference between the two wings and the core of the anticline reaches 300 m (Fig. 8(c)). Oriented nearly NE-SW, the Huangguashan anticline features a dip angle of  $30^{\circ}$  in the

northwest wing and 28° in the southeast wing, resulting in a symmetrical anticlinal structure. The exposed strata in the core consist of the Upper Triassic Xujiahe Formation (Wang et al., 2021). Within the core of the anticline, a fault is present near the northwest wing, which has caused displacement in the Jialingjiang Formation, Leikoupo Formation, and Xuijahe Formation. On the wings. the predominant exposed strata are the Jurassic Zhenzhuchong Formation, Ziliuiing Formation, Xintiangou Formation, and Shaximiao Formation. Huangguashan belongs to the Yongchuan block, situated at the center of the Kaijiang-Luzhou paleo-uplift and within the east Sichuan fault-fold zone. It exhibits a structural pattern characterized by "two depressions and one uplift". The overall structure represents a northeast-oriented long-axis anticline. The axis of the anticline sequentially exposes the Lower Triassic Feixianguan Formation and Jialing River Formation. Furthermore, it can be further divided into five secondary structures: the northern syncline area (burial depth 3700-4200 m), the southern syncline area (burial depth 3850-4150 m), the holding fault block area (burial depth 3850–4050 m), the uplift fault block area (burial depth 3750-3950 m), and the anticline deformation area (Duan and Chen, 2020). Although the Yongchuan block has experienced several large structure movements, large faults are not developed, and large dip angles exist locally. Affected by the paleostructure during deposition and the later multi-stage structure movements, small faults and low-amplitude structures are developed (Liu et al., 2023a), and the amplitude of low-amplitude structures is generally not more than 20 m. According to the causes of formation, the micro structures in the study area can be classified into two categories. The first category is typically influenced by paleogeomorphology, differential compaction, and sedimentary environments. Under the influence of differential

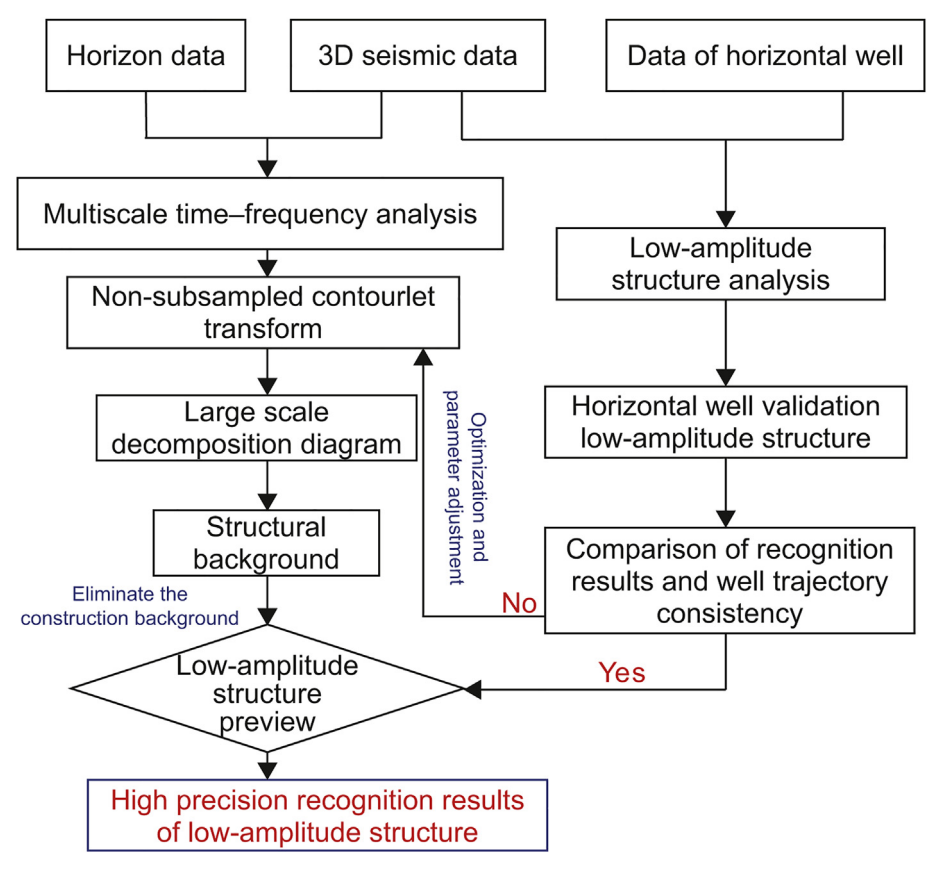


Fig. 7. The low-amplitude structure recognition workflow proposed in this research.

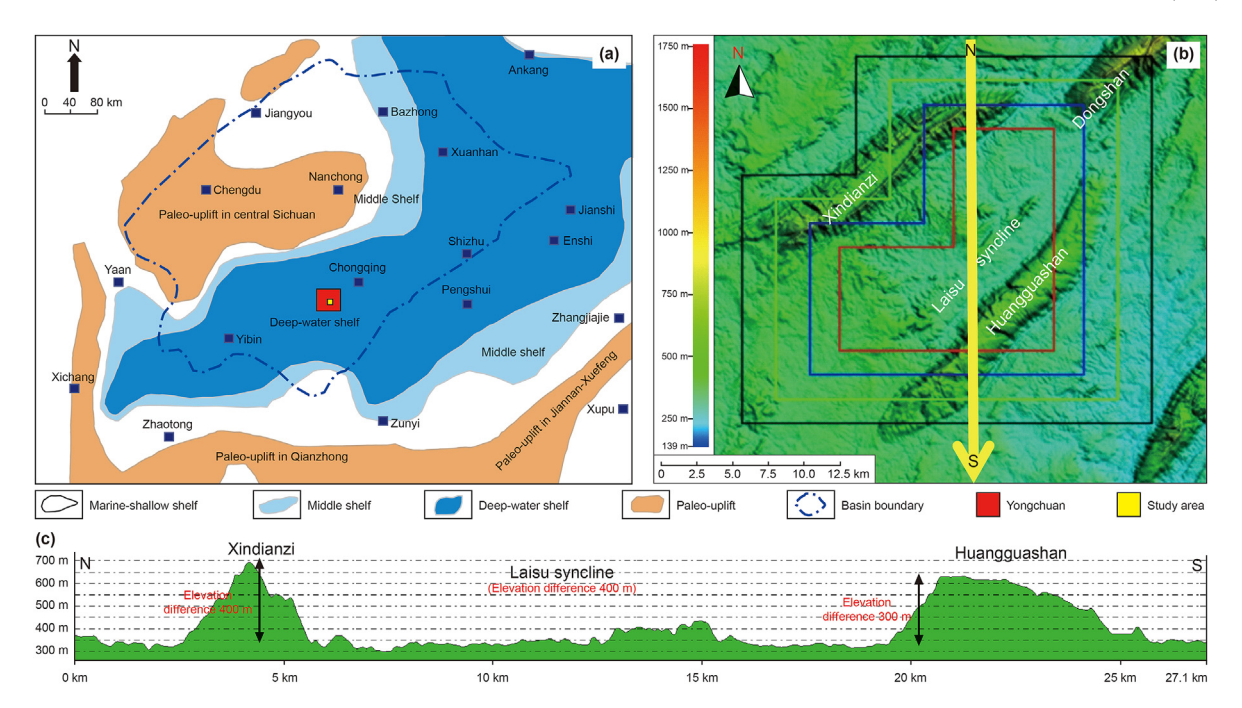


Fig. 8. Geological characteristics of the actual study area. (a) Location map of the study area (modified according to Zhu, 2020). (b) Plane structure diagram (DEM data volume of the study area). (c) Crossline elevation model map of the work area.

compaction, they exhibit either negative or positive low-amplitude structural features. The second category is usually caused by tectonic movements, such as those induced by faults. When the upper plate experiences uneven force distribution, it forms concave structures under stronger stress and convex structures under weaker stress. Research findings indicate that the low-amplitude structural morphology in the study area mainly manifests as positive types (micro-nasal shapes, micro-fault noses, and micro-anticlines) and negative types (micro-grooves, micro-fault grooves, and micro-synclines).

The deep shale gas in Yongchuan Block takes Wufeng-Longmaxi Formation as the target layer, which is overall gentle deep-water shelf facies (Fig. 8(a)). The lithology is mainly gray-black siliceous shale, gray shale, clay shale, and silty shale, with stable horizontal shale development (Huang et al., 2020). Meanwhile, it is subdivided into four types of microfacies: carbon-bearing argillaceous deepwater shelf, graptolite-bearing argillaceous deep-water shelf, bioclastic-lime argillaceous deep-water shelf, and radiolarianbearing argillaceous deep-water shelf. Among them, the dominant microfacies are mainly distributed in the middle and lower part of the Wufeng-Longmaxi Formation, with the total organic carbon content (TOC) ranging from 1.5% to 3.0%, the average gas content of 3.61 m<sup>3</sup>/t, the reservoir pressure of about 70 MPa, the ground pressure coefficient ranging from 1.77 to 1.80, the reservoir temperature of about 130 °C, and the geothermal temperature gradient of 2.70 °C/100 m, which is a high-pressure dry gas reservoir with good gas content (Xie et al., 2019).

We have performed accurate horizon tracing of the bottom of the Wufeng Formation in the study area (global  $5 \times 5$ , well passing area  $1 \times 1$ ), and obtained a horizon structure map with a work area of about  $180 \text{ km}^2$ . Based on this, we have compared and analyzed the low-amplitude structure identification results of the three low-frequency reduction methods with the actual 3D seismic data. Finally, we combined with the horizontal well verification technique, i.e., the variation characteristics analysis using multiple logging values such as TOC values and GR values to guide the accuracy of low-amplitude structure identification.

### 3.2. Comparison in de-low frequency structure mapping

Employing the concept of de-low frequency, we utilize wavelet transform, curvelet transform, and NSCT to depict low-amplitude structures into maps. It is essential to highlight that during the implementation of the wavelet frequency division method, a meticulous selection of the wavelet basis function is imperative. The process involves performing 2D wavelet transform on the constructed data to generate a 2D scale time-frequency map. Subsequently, the wavelet inverse transform is applied to derive a low-amplitude structure map based on wavelet decomposition. Simultaneously, when employing the NSCT method for low-amplitude structure recognition, the complexity of calculation hinges on the filter composition of NSP and NSDFB, necessitating careful consideration in filter selection.

Fig. 9(b)—(d),(f) illustrate a comparison of the low-frequency components decomposed by wavelet transform, curvelet transform, and NSCT, respectively. These components primarily capture the fundamental characteristics of the regional structure. Upon closer examination of the figures, it becomes evident that all three methods exhibit a consistent macro trend in representing the structure. However, notable local variations exist among them. By considering both the contour patterns and depth values, it is apparent that the wavelet transform produces the most distinct deviation from the original structure.

Fig. 9(c)–(e),(g) depict the structural details of the three methods subsequent to the removal of low-frequency background (residuals with the original structure), i.e., the results of recognizing low-amplitude structures. Negative residual values correspond to depression, while positive residual values correspond to uplift. Overall, the low-amplitude structure recognition results from Fig. 9(c)'s wavelet transform and Fig. 9(e)'s curvelet transform exhibit relatively consistent resolution, primarily reflecting larger or overall structural variations. The low-amplitude structure is difficult to identify. The closure height of the wavelet transform recognition result is approximately 80 m, and that of the curvelet transform recognition result is about 50 m, significantly surpassing

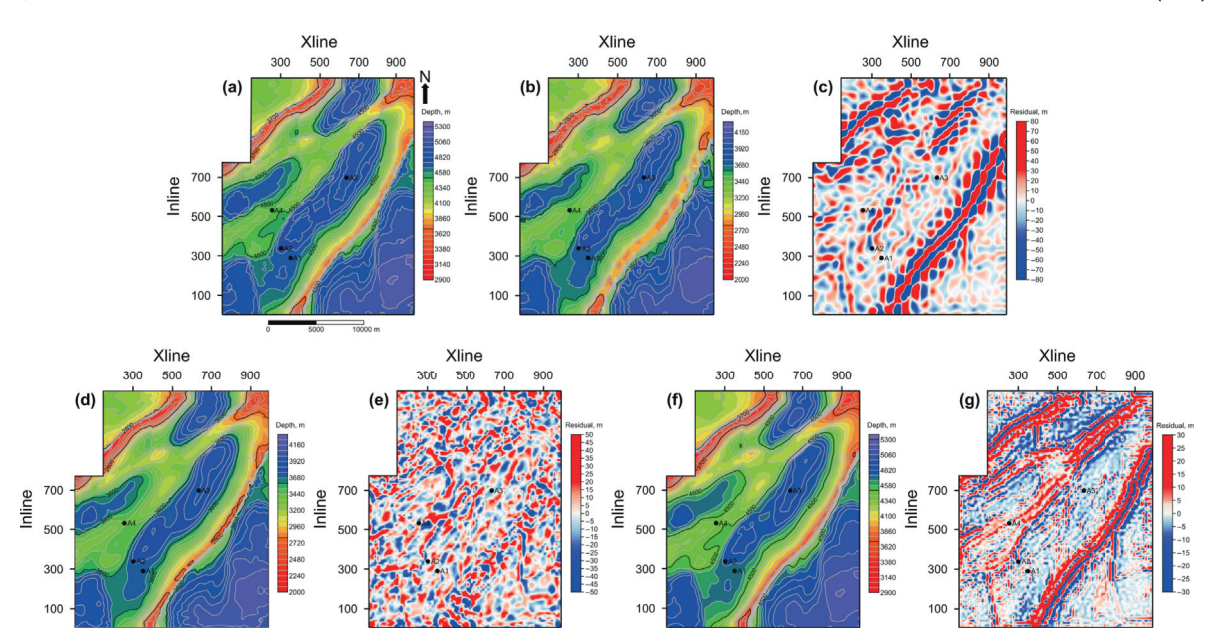


Fig. 9. Comparison of the regional background structures: (b), (d), (f) and the corresponding low-amplitude structures (c), (e), (g) obtained by decomposing (a) the original structure horizon using wavelet transform, curvelet transform, and NSCT.

the closure height of the confirmed low-amplitude structure in the actual work area. Notably, the resolution of the NSCT results in Fig. 9(g) is markedly enhanced, enabling the reflection of small uplift and depression structures, aligning with the recognition of the proven low-amplitude structure closure height within 20 m in the actual work area. Therefore, to further analyze the reliability of the methods, we proceed to conduct a comprehensive comparison and validation by integrating seismic data and horizontal well data from the actual working area.

#### 3.3. Comparison in horizontal well

To conduct a more comprehensive and accurate comparison of the three de-low-frequency methods in identifying low-amplitude structures, we integrate horizontal well data and seismic profiles from the study area for analysis. By examining the cross-well seismic profiles along the well trajectory, multiple low-amplitude structures located at the bottom horizon of the Wufeng Formation in the horizontal well area are identifiable. Meanwhile, in order to more comprehensively compare the identification effects of the three methods in different structural backgrounds, we selected four horizontal wells according to the complexity of the geological situation: The horizontal section of well A1 extends 1500 m (4290-5790 m) in a direction of 42°, and the target layer is the Wufeng Formation of the Ordovician. The structural position belongs to a part of the Yangtze quasi-platform Chongqing platform flexure. The actual drilling data is generally consistent with the seismic data trend, indicating an overall downward dip of the stratigraphy with some noticeable differences. Local rapid changes in the stratigraphy occur, making the geological structure relatively complex. The comprehensive quality evaluation of logging indicates that the Class I reservoir in the horizontal section of A1 well spans 1313.8 m (87.6%). The horizontal section of well A2 is 1500 m long, with a trajectory direction from the starting point to the endpoint at 226°, and the target layers are the Longmaxi and Wufeng Formations. The structural location is in the southern section of the Laisu syncline. The overall dip of the target layer is upward, and the actual drilling trajectory indicates that the horizontal section of the well has a complex structure, consisting of a

fold belt, a transition zone, a horst, and a steepening belt from the starting point to the endpoint. The horizontal section of well A3 extends 1500 m in a direction of 42°, and the target layer is the Ordovician Wufeng Formation. The structural location is the slope between Huangguashan structure and Laisu syncline. The overall dip of the target layer slopes upwards, and the horizontal section is generally flat with local folds. The angle of stratum dip changes from  $2^{\circ}$  upward to  $2^{\circ}$  downward, but the actual stratum dip between 5200 and 5900 m is 5°-7° upward, which differs significantly from the seismic trend. The horizontal section of well A4 is 1500 m long, with a trajectory direction from the starting point to the endpoint at 223°, and the target layers are the Longmaxi and Wufeng formations. The structural location is at the southwestern end of the Dongshan structure. The overall dip of the horizontal section is downward, with a wave-like shape and significant undulations due to stress compression, resulting in rapid changes in the stratigraphy and local development of small folds. The integrated quality evaluation of logging shows that the Class I reservoir of the A4 horizontal section is 1451.0 m, with a proportion of 68.0%. In conclusion, the overall stratigraphy of the horizontal Sections A1 and A3 is relatively gentle, whereas the stratigraphy of the horizontal Sections A2 and A4 exhibits more significant undulations.

As shown in Fig. 10, the recognition results of the three methods over the A1 horizontal well trajectory are shown along the profile. The planar graph is the residual between the low-frequency background and the original structural data, the blue line in the profile represents the horizontal well trajectory, and the green line is the original horizon data. Fig. 10(a) shows the wavelet transform recognition results. In the planar graph, positive residual values represent small anticline structures, while negative residual values represent small syncline structures. By comparing the original horizons of the seismic profile along the well trajectory with the low-frequency horizons of wavelet decomposition, it can be noted that the wavelet transform method can effectively recognize three low-amplitude structures (marked ①, ②, and ③ in the figure), including one small syncline and two small anticlines. Fig. 10(b) shows the results of the curvelet transform, which can effectively recognize three low-amplitude structures, including two small anticlines and one small syncline, with almost the same resolution

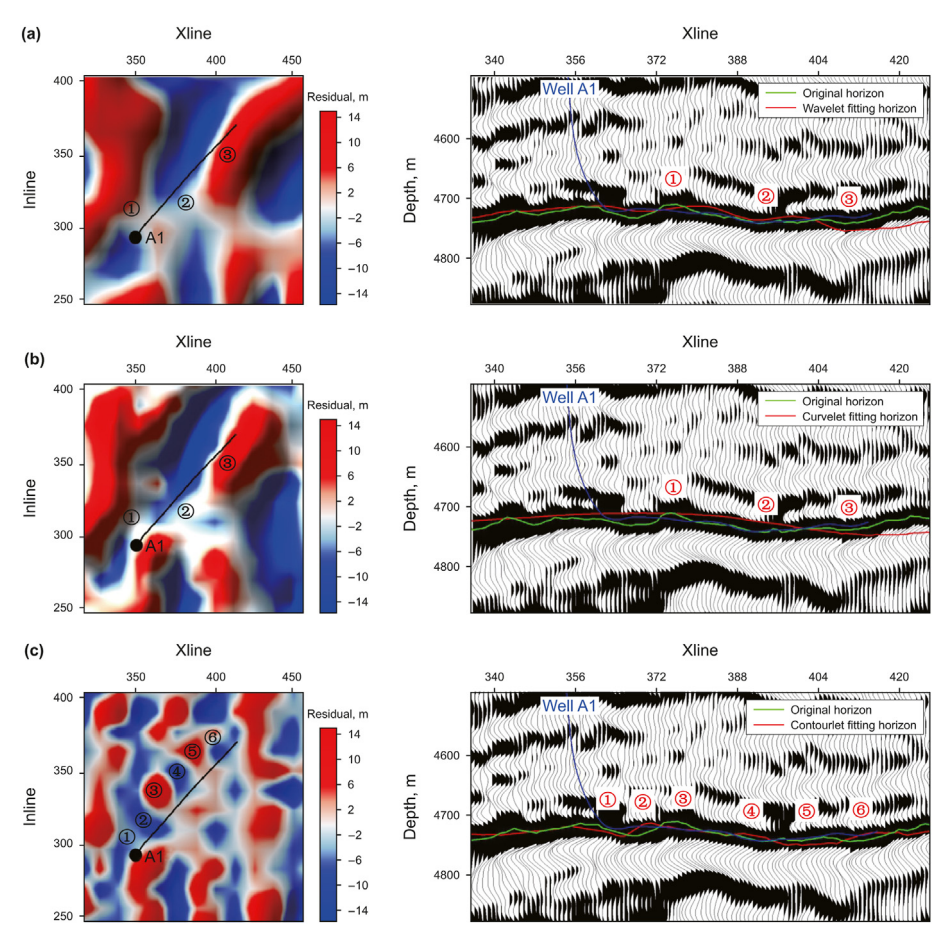


Fig. 10. Comparison of (a) wavelet transform, (b) curvelet transform, and (c) NSCT recognition results along the well trajectory plane and seismic profile of horizontal well A1 in the study area.

as the wavelet transform. Fig. 10(c) shows the results of NSCT recognition, which can effectively identify six low-amplitude structures, including three small anticlines and three small synclines, and the low-frequency results of decomposition are better fitted with the original horizon than the previous two methods, and the resolution of low-amplitude structure recognition is also improved. We analyze that it is because the NSCT uses a nonsubsampling operation to make the decomposed structure image with displacement invariant, multi-scale and multi-directional characteristics. Compared to curvelet and wavelet transforms, NSCT not only preserves fine details but also exhibits enhanced capability in distinguishing high-frequency noise from useful signals, thereby improving the recognition rate of subtle structures. Furthermore, NSCT possesses advantages such as rotation invariance, local singularity, and robustness against noise, enabling better handling of complex image structures and enhancing the ability to finely identify low-amplitude structures.

Similarly, according to the well crossing seismic profile along the well trajectory, multiple low-amplitude structures can be identified on the horizon of the Wufeng Formation bottom in the A3 well area, as depicted in Fig. 11. Through wavelet transform, two low-amplitude structures can be discerned, while curvelet analysis identifies three, and the NSCT detects four such structures. Notably, the curvelet exhibits slightly higher resolution compared to the wavelet transform, whereas the NSCT demonstrates the highest resolution. Furthermore, upon comparing the results with the plane map, it becomes evident that the NSCT recognition yields the most detailed distribution. The recognition results of wells A1 and

A3, where the strata of the over-well trajectory are relatively gentle, show that the number of low-amplitude structures identified by the NSCT is much higher than that of the wavelet and the curvelet transform, indicating that the wavelet and curvelet transform are difficult to identify micro-relief structures. In contrast, the NSCT displays greater sensitivity towards such features.

Using the same method, multiple low-amplitude structures can be recognized on the bottom of the Wufeng Formation in the A2 well area based on the cross-well seismic profile along the well trajectory, as shown in Fig. 12. Four structures can be identified by wavelet transform, four by curvelet transform, and six by NSCT. The recognition results of well A2 in both the plane and profile suggest that the recognition resolution of the curvelet transform appears to be higher than that of the wavelet transform. We believe that this may be due to the appropriate selection of wavelet basis functions at this location, which effectively captures high-frequency details in low-amplitude structures. In contrast, the curvelet transform usually employs curve-shaped basis functions with relatively wide frequency domain characteristics, leading to relatively lower resolution at this location. Moreover, the curvelet transform may be more sensitive to noise and interference signals at this location. resulting in lower local resolution. NSCT identifies low-amplitude structures with the highest accuracy compared to the three methods and is clearly shown on the surface map.

According to the cross-well seismic profile along the well trajectory, multiple low-structures can also be identified on the horizon of the Wufeng Formation bottom in the A4 well area, as shown in Fig. 13, four can be identified through wavelet transform,

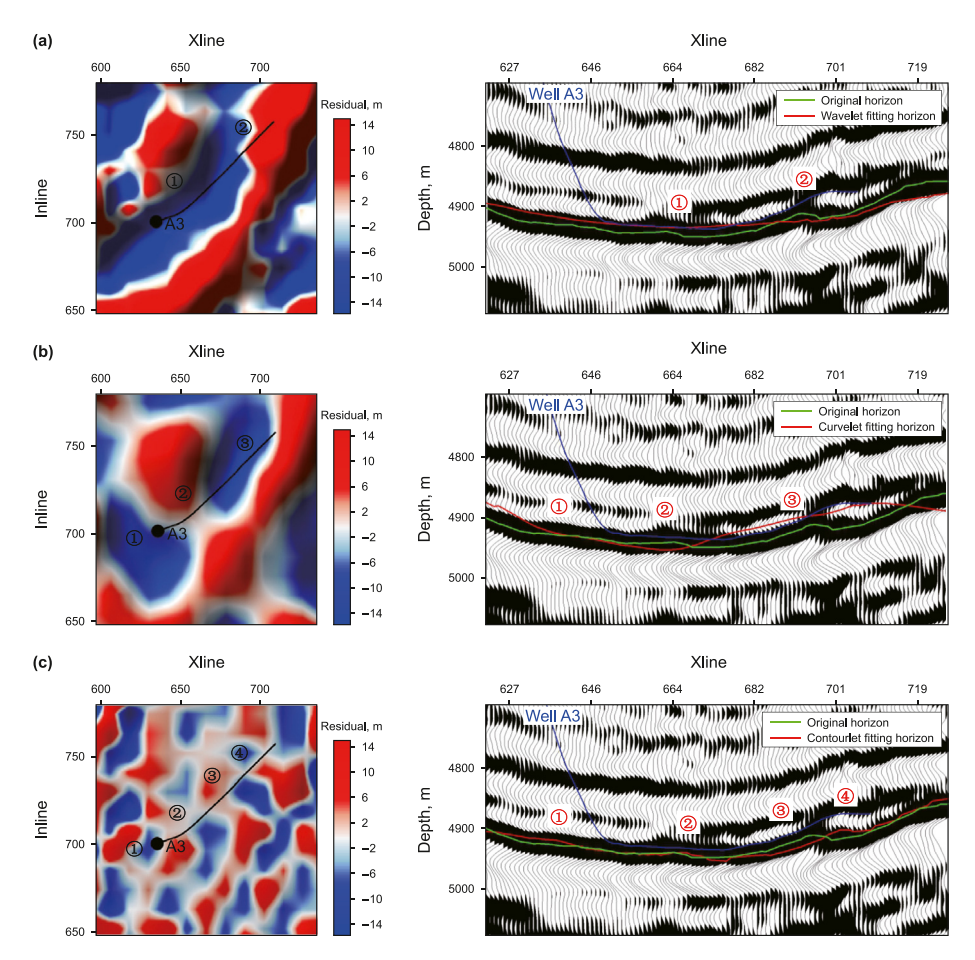


Fig. 11. Comparison of (a) wavelet transform, (b) curvelet transform, and (c) NSCT recognition results along the well trajectory plane and seismic profile of horizontal well A3 in the study area.

four can be identified through curvelet, and six can be identified through NSCT. The same shows that the NSCT recognition results have the highest resolution. Through the recognition results of A1 and A3 wells with relatively large stratigraphic fluctuations in the well trajectory, it can be seen that although the number of lowamplitude structures identified by NSCT is more than that of wavelet and curvelet transform, the difference is smaller, which indicates that the three methods can identify the low-amplitude structures with slightly larger differences in stratigraphic structure height, and the NSCT recognition accuracy is still the highest. Therefore, combining the four wells with different geological conditions, it can be found that the NSCT recognition accuracy is the highest for both low-amplitude structures with large differences in structural elevation, i.e., large scale, and low-amplitude structures with small undulations, i.e., small scale, indicating that our proposed method is applicable in different geological complexity situations.

Taking the structures ② and ③ of the seismic profile crossing the well A4 as an example, the fitting results of the three methods are intuitively compared and displayed.

Based on the analysis of Fig. 14, it is evident that both the wavelet transform and curvelet transform methods provide relatively accurate low-frequency separation. These methods effectively fit the target horizons and successfully separate the localized "small folds". However, the "low frequency volume" generated by these two methods is limited by their fitting accuracy, resulting in interconnected local "small folds" and consequently compromising the resolution of low-amplitude structure identification. In

contrast, the NSCT fitting produces a residual plane map with higher resolution, thereby facilitating the identification of low-amplitude structures within the study area. Consequently, the NSCT method is recommended as the preferred approach for recognizing low-amplitude structures in practical applications.

# 3.4. Horizontal well verification

When utilizing horizontal well guidance to validate the interpretation results, 3D seismic data can assist in judging macroscopic structures. However, due to the weak seismic response of lowamplitude structures, they are often susceptible to noise interference, making it challenging to accurately depict features such as small faults, uplifts, and folds solely based on seismic interpretation results. Moreover, incorrect judgments of wave impedance interfaces during interpretation can introduce false structures into the results, causing deviations between actual drilling trajectories and expectations, ultimately reducing the probability of drilling into high-quality reservoirs (Liu et al., 2022b). Therefore, to further analyze and verify the method's advantages, we validate the lowamplitude structure recognition results based on real drilled wells. Using logging curves such as TOC, GR, and well deviation, we analyze various parameter values and morphological change characteristics to identify the real drilled low-amplitude structures, determine the real structure type, check the false structures in the identification results based on the proposed method, and finally analyze the location of high-quality reservoir distribution, at the same time, lay the foundation for horizontal well trajectory

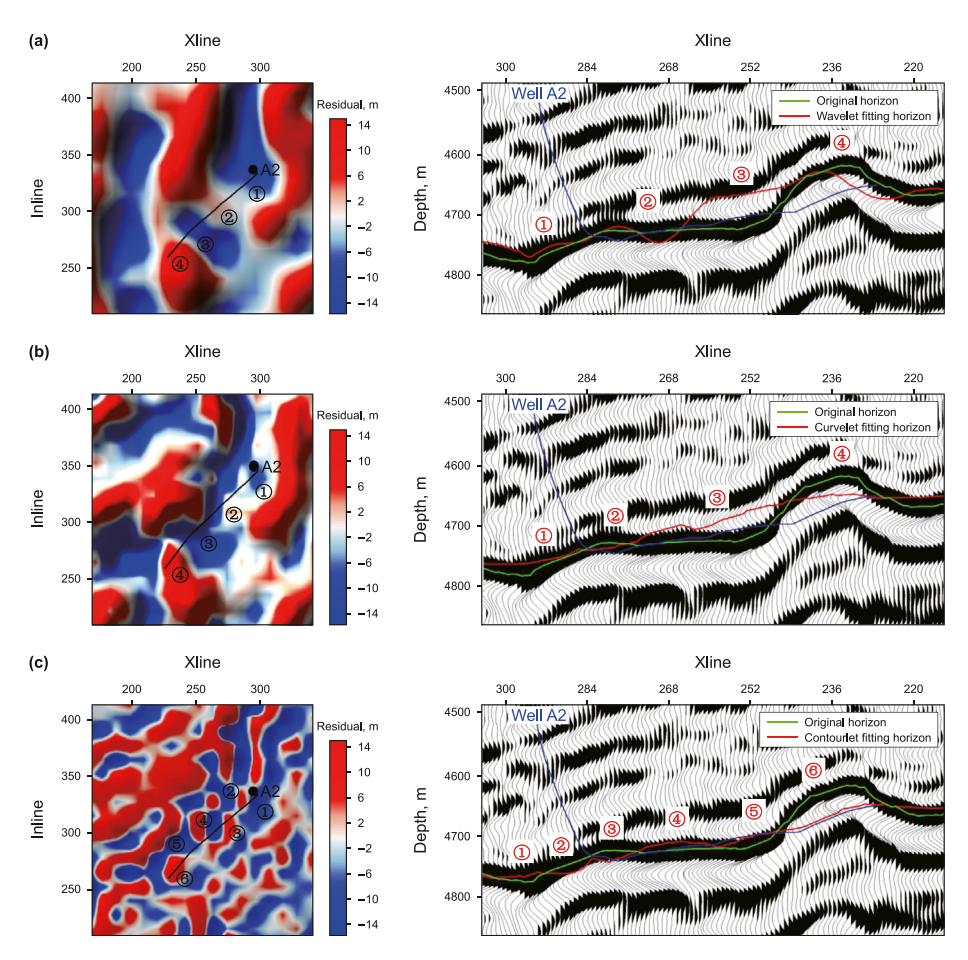


Fig. 12. Comparison of (a) wavelet transform, (b) curvelet transform, and (c) NSCT recognition results along the well trajectory plane and seismic profile of horizontal well A2 in the study area.

optimization.

GR is the natural gamma curve, which is usually used to analyze the shale content. At the same time, TOC represents the total organic carbon content, which is generally used to characterize the gas content and hydrocarbon generation capacity of shale, and is regarded as the critical parameter of the "geological sweet spot", and usually when its content is higher than 2% (Xiao et al., 2023), it means the shale has basic hydrocarbon generation capacity.

As shown in Fig. 15, during the actual drilling process, the horizontal well trajectory curve is basically consistent with the stratigraphic dip angle of the seismic profile, which indicates that the structure of the seismic profile crossing the horizontal well is basically consistent with the actual drilling, and can reflect the structural characteristics of the bottom of the Wufeng Formation more truly. The sudden drop of GR and TOC can indicate that the horizontal well meets the "small uplift" structure, and the false structure can be corrected in time through this feature. By collecting actual drilling and logging parameters, three small anticline structures are verified in the horizontal well A1 in Fig. 15(a), which is consistent with the recognition results of the NSCT method. Two small anticline structures are identified by wavelet transform, and two small anticline structures are identified by curvelet transform. The advantages of the NSCT method are apparent. Meanwhile, in Fig. 15(b), through manual identification of GR and TOC sudden drop sections, two small anticline structures are identified in horizontal well A2, two small anticline structures are identified in horizontal well A3 in Fig. 15(c), and four small anticline structures are identified in horizontal well A4 in Fig. 15(d), which is consistent

with the recognition results of NSCT-based method. However, two small anticline structures are identified by wavelet and curvelet transform-based approaches. In order to demonstrate the effectiveness of the NSCT method more intuitively, we extract the GR and TOC well logging curves from well A1 and display them on the same profile as the original stratigraphic and NSCT fitted curves (see Fig. 16). It can be observed that there are three significant drops in the well curves, which align with the identification of three small anticlines by the NSCT analysis. In summary, combined with the actual well curve verification, low-amplitude structure recognition results by using NSCT are almost consistent with the actual drilling, which proves that the proposed method is reliable and provides technical support for the optimization and deployment of drilling trajectories in the later stage and adjacent wells.

In this section, we extract pertinent logging parameters to validate the accuracy of identifying low-amplitude structures based on the actual drilling trajectories of horizontal wells. The results of low-amplitude structure identification are derived from decomposing the low-frequency background using multi-scale time-frequency analysis methods. In comparison with the cross-well seismic profiles, the "low-frequency model" constructed by the wavelet and curvelet transform can be well differentiated from the original stratigraphy. However, the performance is insufficient and suitable for identifying "structural ridge" in the study area. Both methods have a low degree of fitting with actual drilling trajectories. The highly directional and anisotropic NSCT is more appropriate for low-amplitude structure recognition. The result of the proposed method matches better than that of the traditional

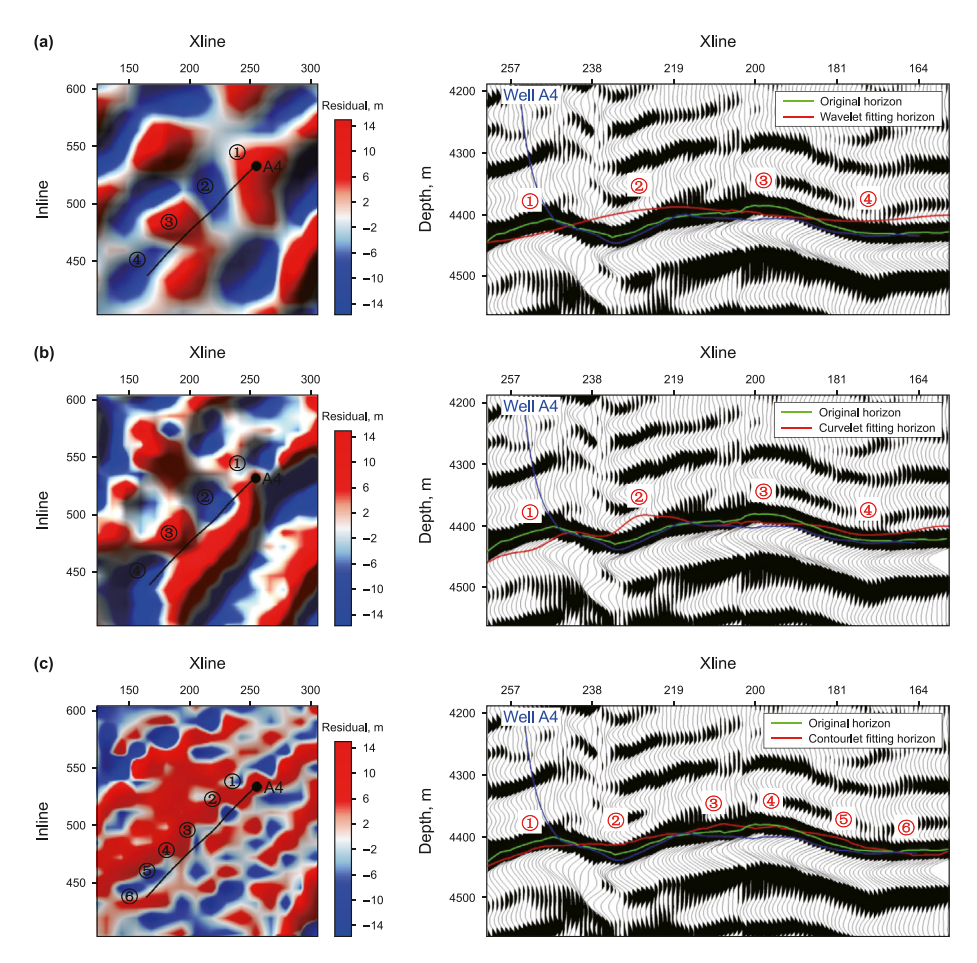


Fig. 13. Comparison of (a) wavelet transform, (b) curvelet transform, and (c) NSCT recognition results along the well trajectory plane and seismic profile of horizontal well A4 in the study area.

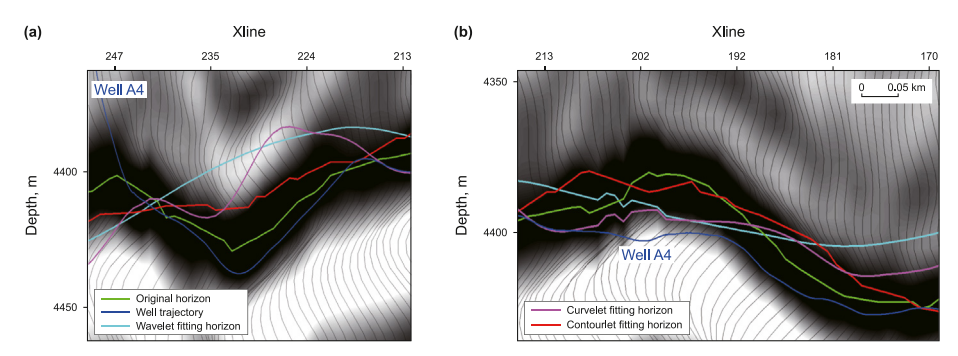


Fig. 14. Comparison of fitting degrees of three methods for crossing the well A4 seismic profile in the study area at (a) ② syncline structure and (b) ③ anticline structure. The results obtained from the wavelet transform method exhibit the lowest fitting degree, followed by the curvelet transform method. The NSCT identification results demonstrate the highest fitting degree among the three methods.

wavelet transform and curvelet transform. It can more comprehensively capture structural features in all directions of the structural plane, providing richer structural information for reconstruction after separation. The final step is to verify the low-amplitude structure recognition results by combining horizontal wells, using various logging data such as TOC, GR, etc., to analyze the change characteristics. It can be found that the NSCT-based low-amplitude structure identification results are basically consistent with the actual drilling and more suitable for recognizing low-amplitude structures in the study area. Fig. 9(g) shows the final low-amplitude structure identification surface of the target layer in

the study area, where high residual values represent positive low-amplitude structures and low values indicate negative low-amplitude structures. The low-amplitude structures are mainly developed near large anticlines. Meanwhile, three-dimensional identification of local low-amplitude structures near the drilling platform in the research area reveals that the amplitude difference around the well generally does not exceed 3 m. Although small folds exist, the terrain is relatively gentle compared to the whole work area. Therefore, studying low-amplitude structures provides a foundation for selecting well locations.

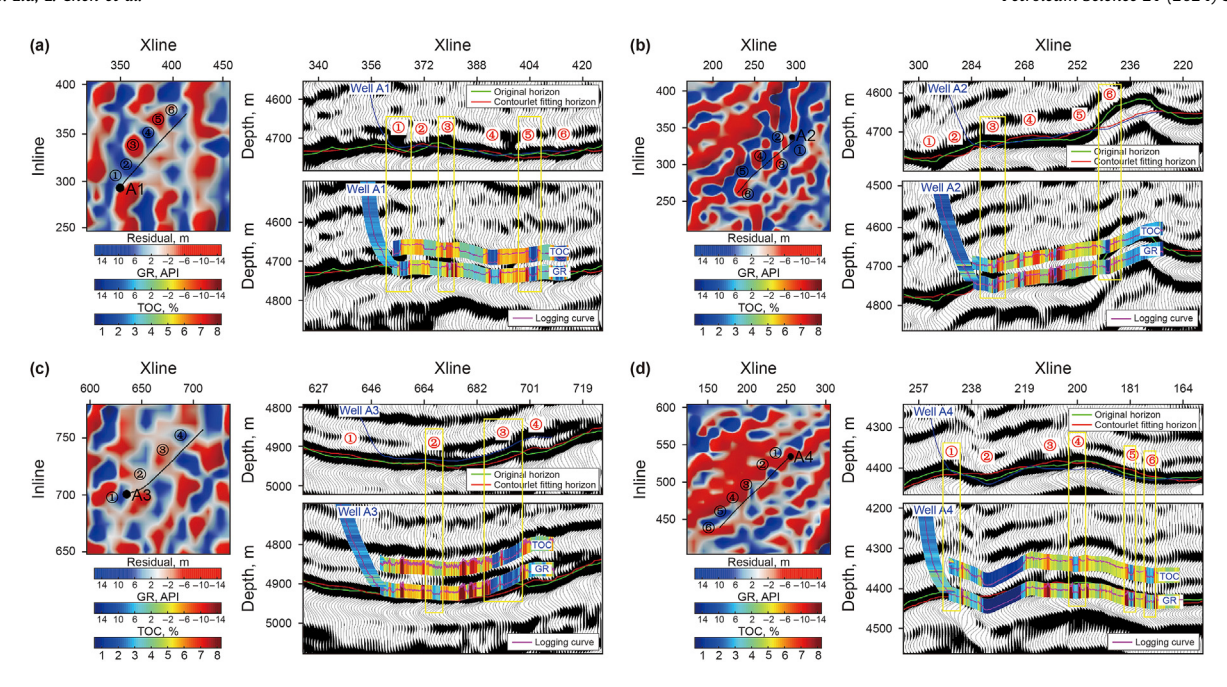
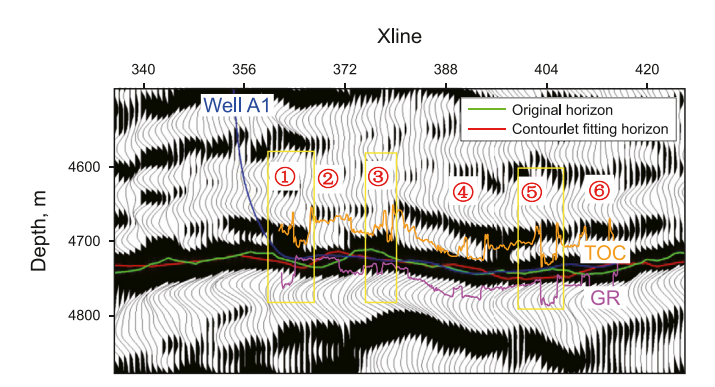


Fig. 15. Validation of the low-amplitude structure recognition results, i.e., the low-amplitude structure recognition plane and logging curve feature profile of horizontal wells (a) A1, (b) A2, (c) A3, and (d) A4.



**Fig. 16.** Comparison of low-amplitude structure recognition results with TOC and GR logging curves in well A1.

#### 4. Conclusion

In summary, we propose a process and method for identifying low-amplitude structures based on time-frequency analysis. The large-scale analysis obtained through time-frequency transformation preserves the low-frequency background of the structures, while the small-scale analysis reveals the structural details. This approach ensures both structural continuity and local focus in the identification results. It fully utilizes the redundant properties of scale in time-frequency analysis to achieve a multi-scale decomposition of the two-dimensional image of the structural interpretation. Building upon this, we develop a method for precise identification of low-amplitude structures based on NSCT. This method captures the characteristics of low-amplitude structures in multiple directions and scales, allowing for accurate identification of these structures through reconstruction. Validation through horizontal wells, as well as the comparison of logging parameters such as TOC and GR values, confirms that the results of the proposed method align closely with actual drilling data. Through various comparisons, it is evident that the NSCT exhibits significant advantages in identifying low-amplitude structures. It effectively separates regional background from local low-amplitude structures, enhances the features of local microstructures, and highlights them on the structural plane map. This demonstrates the effectiveness and superiority of using NSCT for identifying low-amplitude structures. The practical application of this method in work areas provides a reliable basis for well-location deployment.

## **CRediT authorship contribution statement**

**Fen Lyu:** Conceptualization, Data curation, Investigation, Methodology, Software, Writing — original draft. **Xing-Ye Liu:** Conceptualization, Methodology, Resources, Validation, Writing — review & editing. **Li Chen:** Data curation. **Chao Li:** Formal analysis, Validation. **Jie Zhou:** Writing — review & editing. **Huai-Lai Zhou:** Investigation, Validation.

### **Declaration of competing interest**

The authors declare that they have no known competing financial interests or personal relationships that could have appeared to influence the work reported in this paper.

# Acknowledgments

The authors sincerely thank Chongqing Gas Field of PetroChina Southwest Oil & Gas Field Company management for granting permission to present this paper and seismic datasets. This work is supported by Sichuan Science and Technology Program under Grant 2024NSFSC1984 and Grant 2024NSFSC1990

### References

Asmare, M.H., Asirvadam, V.S., Hani, A.F.M., 2015. Image enhancement based on contourlet transform. Signal. Image and Video Processing 9, 1679—1690. https://doi.org/10.1007/s11760-014-0626-7.

Bai, X.Y., Guo, J.J., Chen, Y.B., 2011. Application of S-transformation to recognition of low-amplitude structure: an example from Lu 10–Lu 6 well area in hinterland of Junggar Basin. Lithologic Reservoirs 23 (5), 83–86. https://doi.org/10.3969/ i.issn.1673-8926.2011.05.018.

Candes, E.J., Donoho, D.L., 1999. Curvelets: a surprisingly effective nonadaptive representation for objects with edges. Stanford: Department of Statistics.

#### Stanford University.

Candes, E.J., Donoho, D.L., 2010. New tight frames of curvelets and optimal representations of objects with piecewise C2 singularities. Commun. Pure Appl. Math. 57 (2), 219–266. https://doi.org/10.1002/cpa.10116.

- Chai, T., Bi, M.B., 2019. Application of the technology of trend surface analysis in the process of recognizing the low amplitude structural oil and gas reservoir—taking the Tian Huan depression in Ordos basin as an example. Journal of Xian University (Natural Science Edition) 22 (1), 90–93.. CNKI:SUN: XAIY.0.2019-01-020.
- Cunha, A.L., Zhou, J.P., Do, M.N., 2005. Nonsubsampled contourlet transform: filter design and application in denoising. IEEE International Conference on Image Processing, Genoa, pp. 749–752.
- Cunha, A.L., Zhou, J.P., Do, M.N., 2006. The nonsubsampled contourlet transform: theory, design, and applications. IEEE Trans. Image Process. 15 (10), 3089—3101. https://doi.org/10.1109/tip.2006.877507.
- Do, M.N., Vetterli, M., 2002. Contourlets: a new directional multiresolution image representation. In: Conference Record of the Thirty-Sixth Asilomar Conference on Signals, Systems and Computers, vol. 1. IEEE, pp. 497–501. https://doi.org/ 10.1109/ACSSC.2002.1197232
- Donoho, D.L., 1995. De-noising by soft-thresholding. IEEE Trans. Inf. Theor. 41 (3), 613–627. https://doi.org/10.1109/18.382009.
- Duan, G.B., Chen, C.G., 2020. Study of reservoir forming conditions of deep shale gas in the west Chongqing block. Acta Geol. Sichuan 40 (3), 402–405. https://doi.org/10.3969/j.issn.1006-0995.2020.03.011.
- Emmanuel, J.C., Donoho, D.L., 2000. Curvelets-A surprisingly effective nonadaptive representation for objects with edges. curve & surface fitting. https://doi.org/ 10.1086/116933.
- Fang, C.J., Zeng, Y.J., Kong, L.H., 2010. Identification method for low amplitude structure in foreland basin slope zone, a block of south America. Oil Geophys. Prospect. 45 (S1), 134–136+240+254. https://doi.org/10.13810/j.cnki.issn.1000-7210.2010.s1004
- Ge, Y.H., Kang, Z.J., 2008. Weighted technology of moving trend surface fitting. J. Eng. Graph. (2), 110–114. https://doi.org/10.3969/j.issn.1003-0158.2008.02.019.
- Grossmann, A., Morlet, J., 1984. Decomposition of hardy functions into squareintegrable wavelets of constant shape. SIAM J. Math. Anal. 15 (4), 723–736. https://doi.org/10.1137/0515056.
- Herrmann, F.J., Wang, D., Hennenfent, G., et al., 2008. Curvelet-based seismic data processing: a multiscale and nonlinear approach. Geophysics 73 (1), A1–A5. https://doi.org/10.1190/1.2799517.
- He, Y.W., Chen, G.F., 2020. Micro-amplitude structure identification method and its application in X105 block. Journal of Southwest Petroleum University (Science & Technology Edition) 42 (3), 43–50. https://doi.org/10.11885/j.issn.1674-5086.2018.10.23.01.
- Hu, J.Z., Zhang, W.T., Hu, R.Q., et al., 2019. The application of layered fitting to obtain layer velocity field construction technology in low amplitude structure identification. In: 2019 Symposium on Geophysical Prospecting Technology of China Petroleum Institute, pp. 653–656.
- Hu, Y.S., Zhang, H.L., Li, Z.D., et al., 2012. Recognition of tiny amplitude structure of exploration seismic in the application of first district of eastern south central block in Lamadian oilfield. Sci. Technol. Eng. 12 (4), 735–739.
- Huang, H., Li, R., Jiang, Z., et al., 2020. Investigation of variation in shale gas adsorption capacity with burial depth: insights from the adsorption potential theory. J. Nat. Gas Sci. Eng. 73, 103. https://doi.org/10.1016/j.jngse.2019.103043, 043
- Jiang, C.J., Jiang, H.L., Zhao, F.H., 2005. Micro-range structure and lithologic traps identification technique and its application. Pet. Geol. Oilfield Dev. Daqing 24 (3), 19–20. https://doi.org/10.3969/j.issn.1000-3754.2005.03.007.
- Lancaster, P., Salkauskas, K., 1981. Surfaces generated by moving least squares methods. Math. Comput. 37 (155), 141–158. https://doi.org/10.2307/2007507.
- Li, G.C., Dai, W.J., Zeng, F.H., et al., 2016. Application of three-dimensional dynamic trend Surface fitting model on land subsidence. J. Geodesy Geodyn. 36 (6), 508-511. https://doi.org/10.14075/j.jgg.2016.06.009.
- Liu, X., Chen, X., Cheng, J., et al., 2023a. Simulation of complex geological architectures based on multi-stage generative adversarial networks integrating with attention mechanism and spectral normalization. IEEE Trans. Geosci. Rem. Sens. https://doi.org/10.1109/TGRS.2023.3294493.
- Liu, X., Chen, X., Li, J., et al., 2020. Facies identification based on multikernel relevance vector machine. IEEE Trans. Geosci. Rem. Sens. 58 (10), 7269–7282. https://doi.org/10.1109/TGRS.2020.2981687.
- Liu, X., Cheng, J., Cai, Y., et al., 2022a. Stochastic simulation of facies using deep convolutional generative adversarial network and image quilting. Mar. Petrol. Geol. 146, 105932. https://doi.org/10.1016/j.marpetgeo.2022.105932.
- Liu, X., Shao, G., Liu, Y., et al., 2021. Deep classified autoencoder for lithofacies identification. IEEE Trans. Geosci. Rem. Sens. 60, 1–14. https://doi.org/10.1109/ TGRS.2021.3139931.
- Liu, X., Shao, G., Yuan, C., et al., 2022b. Mixture of relevance vector regression experts for reservoir properties prediction. J. Petrol. Sci. Eng. 214, 110498. https://doi.org/10.1016/j.petrol.2022.110498.
- Liu, X., Zhou, H., Guo, K., et al., 2023b. Quantitative characterization of shale gas reservoir properties based on BiLSTM with attention mechanism. Geosci. Front. 101567. https://doi.org/10.1016/j.gsf.2023.101567.
- Lu, Y., Do, M.N., 2003. CRISP-contourlets: a critically sampled directional multiresolution image representation. Proc. SPIE-Int. Soc. Opt. Eng. 5207. https://

doi.org/10.1117/12.506566.

- Mullineux, G., 2008. Non-linear least squares fitting of coefficients. Appl. Math. Model. 32 (12), 2538–2551.
- Pu, R.H., 1998. An approach of spill point constrained velocity field: a method for improving image accuracy of low closure structures. Oil Gas Geol. 19 (2), 106–108. CNKI:SUN:SYYT.0.1998-02-003.
- Qian, K.R., He, Z.L., Liu, X.W., et al., 2018. Intelligent prediction and integral analysis of shale oil and gas sweet spots. Petrol. Sci. 15 (4), 744–755. https://doi.org/10.1007/s12182-018-0261-v.
- Schonewille, M., Aaron, P., Allen, T., 2007. Applications of time-domain high-resolution Radon demultiple. ASEG Extended Abstracts (1), 1–5. https://doi.org/10.1071/aseg2007ab003.
- Shang, B.Z., Caldwell, D.H., 2003. A bandwidth enhancement workflow through wavelet analysis. In: 2003 SEG Annual Meeting, Society of Exploration Geophysicists. https://doi.org/10.1190/1.1817725.
- Shao, Y., Li, X.Y., Kong, Z.Y., et al., 2003. Study on application of velocity-field model-building method. Oil Geophys. Prospect. 38 (6), 675–679. https://doi.org/10.3321/j.issn:1000-7210.2003.06.016.
- Teng, D.B., Wang, P.C., Wang, Y., et al., 2005. The identification of small faults and low-amplitude structures by utilizing prestack Kirchhoff integral migration. Prog. Geophys. 20 (4), 1035–1038. https://doi.org/10.3969/j.issn.1004-2903.2005.04.025.
- Wang, G., Ni, G.S., et al., 2021. Research and application of down Hole Microseismic Monitoring Adaptability in Huang 202 well area. Adv. Geosci. 11, 1112. https://doi.org/10.12677/AG.2021.118107.
- Wang, S.L., Shi, W., Zhang, B., 2015. Identification method of low amplitude structure in Matouying bump salience. Petrol. Geol. Eng. 29 (5). https://doi.org/10.3969/j.issn.1673-8217.2015.05.002, 5-7+144.
- Wang, X., Liu, W.Q., Zeng, H.H., et al., 2018. Stratified constrained near-surface model building method and its application in complex surface area. Lithologic Reservoirs 30 (5), 68–73. https://doi.org/10.12108/yxyqc.20180508.
- Wu, T., Shi, X.W., Ge, Q.Y., 2022. Seismic data processing technology and application of shale gas in southern Sichuan mountain area. 2022. Annual Symposium of China Petroleum Geophysical Exploration II, 4. https://doi.org/10.26914/ c.cnkihy.2022.039502.
- Wu, Y., Ma, T., Wang, Y., et al., 2017. Multi-parameter analysis of identifying micro amplitude structures by moving trend surface method. Journal of Southwest Petroleum University (Science & Technology Edition) 39 (3), 34–46. https:// doi.org/10.11885/j.issn.1674-5086.2017.01.10.03.
- Xia, H.M., Zheng, X.W., Huang, H.D., et al., 2021. The application of low-amplitude structure based on low-frequency reduction. Geophys. Geochem. Explor. 45 (4), 998–1003. https://doi.org/10.11720/wtyht.2021.1167.
- Xiao, Z., Zhao, J., Zhong, Q., et al., 2023. Anisotropic dispersion mechanism of intersalt shale oil reservoir in terrestrial saline lake sediments using cross-band experiments. Sci. China Earth Sci. 1–19. https://doi.org/10.1007/s11430-022-1063-3.
- Xie, J., Qin, Q., Fan, C., 2019. Influencing factors of gas adsorption capacity of marine organic shale: a case study of Dingshan area, southeast Sichuan. J. Coast Res. 93 (sp1), 507–511. https://doi.org/10.2112/S193-066.1.
- Xu, H.T., Jing, H.L., Chang, Q.L., et al., 2012. Variable velocity mapping method and effect analysis for the complex structure on the south margin of Junggar Basin. Special Oil Gas Reservoirs 19 (2), 50-53+137. https://doi.org/10.3969/j.issn.1006-6535.2012.02.012.
- Xue, L., Gu, S.H., Jiang, X.E., et al., 2021. Ensemble-based optimization of hydraulically fractured horizontal well placement in shale gas reservoir through Hough transform parameterization. Petrol. Sci. 18, 839–851. https://doi.org/10.1007/ s12182-021-00560-3.
- Zhang, J., Huang, Y., 2002. Method for using 2D seismic data for locating low-amplitude traps. China Petroleum Exploration 7 (3), 54–59. https://doi.org/10.3969/j.issn.1672-7703.2002.03.009.
- Zhang, Q., Guo, B.L., 2007. Research on image fusion based on the nonsubsampled contourlet Transform. In: IEEE International Conference on Control and Automation. Guangzhou, pp. 3239–3243.
- Zhao, Z.Y., 1982. Discovery of grouped slight relief structures in a special depression. Geophys. Prospect. Pet. (4), 114–118.
- Zhao, Z.Y., 1987. Groups of structures with micro-amplitudes and the regularity of hydrocarbon accumulation in Sanzhao Sag. Pet. Geol. Oilfield Dev. Daqing 6 (2), 15–22. https://doi.org/10.19597/j.issn.1000-3754.1987.02.004.
- Zheng, X.F., Kong, X.S., Li, Y.C., et al., 2017. Variable-velocity structure mapping for the structure 4 in napu sag. Oil Geophys. Prospect. 52 (Suppl. 1), 55–59. https:// doi.org/10.13810/j.cnki.issn.1000-7210.2017.S1.009.
- Zhou, J.P., Cunha, A.L., Do, M.N., 2005. Nonsubsampled contourlet transform: construction and application in enhancement. In: IEEE International Conference on Image Processing, pp. 469–472. https://doi.org/10.1109/icip.2005.1529789.
- Zhou, W., Xie, H.G., Chen, G., 2006. Discussion on low amplitude trap identification method. Hanjiang Petroleum Science and Technology 16 (3), 4–8. CNKI:SUN: JHSK.0.2006-03-003.
- Zhu, H.T., 2020. Application of true and false tiny-amplitude structure identification technique to shale-gas horizontal wells. Mud Logging Engineering 31 (2), 55–60. https://doi.org/10.3969/j.issn.1672-9803.2020.02.010.
- Zhu, L., Zhang, C., Zhang, Z., et al., 2020. High-precision calculation of gas saturation in organic shale pores using an intelligent fusion algorithm and a multi-mineral model. Advances in Geo-Energy Research 4 (2), 135–151. https://doi.org/ 10.26804/ager.2020.02.03.